EXPERIMENTAL AND ANALYTICAL INVESTIGATION ON MECHANICS OF METAL CUTTING INCLUDING EDGE FORCES

by

BURAK AKSU

Submitted to the Graduate School of Engineering and Natural Sciences
in partial fulfillment of the requirements for the degree of
Master of Science

Sabancı University
Spring 2008

EXPERIMENTAL AND ANALYTICAL INVESTIGATION ON MECHANICS OF METAL CUTTING INCLUDING EDGE FORCES

APPROVED BY:

Assoc. Prof.Dr. Erhan Budak (Thesis Advisor)	…….....
Prof. Dr. Yusuf Menceloğlu	…….....
Assoc. Prof.Dr. Ş.İlker Birbil	…….....
Assoc. Prof.Dr. Bülent Çatay	…….....
Assist. Prof.Dr. Kemal Kılıç	…….....

DATE OF APPROVAL: ……..

EXPERIMENTAL AND ANALYTICAL INVESTIGATION ON MECHANICS OF METAL CUTTING INCLUDING EDGE FORCES

Burak AKSU

Industrial Engineering, Master of Science Thesis, 2008

Thesis Advisor: Assoc. Prof. Dr. Erhan BUDAK

Keywords: Machining, Orthogonal Cutting, Oblique Cutting, Edge Forces

ABSTRACT

Almost every field of industry requires machining in their processes. Products are mass manufactured from a sequence of machining operations in certain amount of time. In this material removal processes metal cutting is the most common one. The main purpose is to shape metals and alloys by using chip formation operations and any improvement in the cycle time will reduce the total cost significantly. Therefore, modeling of the machining operations such as turning and milling is very important in terms of process effectiveness.

In accordance with the technological developments and computer integration, the modeling of the metal cutting processes becomes easier. Depending on the application, machining type may differ; however the basic principles remain the same. In this respect, mechanics and the dynamics of the orthogonal cutting model provide invaluable insight regarding the selection of process parameters. In this thesis, the mechanics of orthogonal and oblique cutting is reviewed using analytical and experimental methods for different materials and process conditions. The results are used in mechanistic modeling of the cutting forces and predicted cutting forces are compared with the experimental results. As an important part of the experimental work, edge forces are also analyzed empirically. The effect of hone radius on the cutting process is investigated, and taken into account in force predictions using an analytical model proposed by Ozlu [20], and promising results are obtained and verified by experiments.

METAL KESME MEKANİĞİ VE KENAR KESME KUVVETLERİNİN DENEYSEL VE ANALİTİK OLARAK İNCELENMESİ

Burak AKSU

Endüstri Mühendisliği, Yüksek Lisans Tezi , 2008

Tez Danışmanı: Doç. Dr. Erhan BUDAK

Anahtar Kelimeler: Talaşlı İmalat, Dik Kesme, Eğik Kesme, Kenar Kuvvetleri

ÖZET

Hemen her sektör imalat süreçlerinde talaşlı imalat tekniklerini kullanmaktadır. Üretilen ürünler bir dizi üretim aşamasından geçerek belli bir sürede üretilmektedir. Bu üretim aşamalarının içerisinde talaşlı imalat en yaygınıdır ve ürün kalitesi göz önüne alındığında önemli bir yere sahiptir. Dolayısıyla, bu süreçte üretim zamanını kısaltmaya yönelik yapılacak modelleme ve eniyileme çalışmaları toplam üretim zamanı, maliyeti ve süreç etkinliği açısından kritik bir rol oynayacaktır.

Teknolojik gelişmelerin süreçlere bilgisayar entegrasyonu ile eş zamanlı olarak ilerlemesi metal kesme süreçlerinin modellenmesini de kolaylaştırmıştır. Operasyon çeşidine bağlı olarak metal kesme teknikleri değişebilse de mekanik olarak dayandığı temeller aynı kalmaktadır. Bu bağlamda dikey kesme yönteminin mekanik ve dinamik incelenmesi karmaşık süreçlerin modellemesinde ve en iyi süreç değişkenlerin belirlenmesinde çok önemli bir bakış açısı sağlayacaktır. Bu tez çalışmasında, dikey ve eğik metal kesme teknikleri farklı malzemeler ve kesme koşullarında deneysel ve analitik olarak incelenmiştir. Deneysel olarak elde edilen sonuçlar, analitik modellemede kullanılmıştır. Bu model sayesinde tahmin edilen kuvvetler deneysel olarak ölçülen kuvvetler ile karşılaştırılmış ve genel olarak hesap edilen değerlerin deney sonuçlarıyla uyum içerisinde olduğu gözlenmiştir. Bu deneysel çalışmanın bir diğer önemli sonucu da kenar kesme kuvvetlerinin deneysel ve analitik olarak incelenmesidir. Özlü'nün [20] çalışmasında geliştirdiği model aracılığıyla elde edilen kuvvetler deneysel sonuçlar ile karşılaştırılmış böylelikle kesici takımlar üzerindeki köşe yuvarlama değerlerinin kesme süreçlerine etkileri de incelenmiştir.

to my wife and family…

ACKNOWLEDGEMENTS

First of all, I would like to thank to my thesis advisor, Dr.Erhan BUDAK for his motivation, encouragement and guidance. His support and invaluable feedbacks were very helpful to finalize my two year work in this thesis.

I am very grateful to my wife Emel. She was always with me during rough times. Without her support, endless love and delicious meals this thesis would not be finished on time. Also, I should thank to my father Hüseyin AKSU, my mother Sibel AKSU and my sweet sister Buket AKSU for their presence and supportive attitudes which made me feel stronger.

In addition, I had chance to work with wonderful friends for two years. Dr. Emre ÖZLÜ, L.Taner TUNÇ and Erdem ÖZTÜRK whom I could call as "colleagues" were very helpful for me and my research. Also, technical support of Mr. Mehmet GÜLER and Mr. Süleyman TUTKUN had a great effect on this work. On the other hand, I would like to express my sincere thanks to my brilliant office mates who made the ambiance of our office enthusiastic. However, two of them were very special for me, Serkan ÇİFTLİKLİ and Mahir YILDIRIM. I spent almost a year being their semi room mate in the name of fellowship of 311. Also, I can not forget the times we spent to build a custom made "fare algorithm" with Nihan ÖZŞAMLI, even though it has different mechanism, I know it works.

CONTENTS

LIST OF FIGURES

CHAPTER 1 INTRODUCTION

Metal cutting is the most common method in material removal processes in today's manufacturing environment. The main purpose is to shape metals and alloys by using chip formation operations such as turning, milling and drilling. As far as the big industries (automotive, aerospace, medical, etc.) concerned, the machining of metals gain importance in terms of production cost, time and part accuracy. In accordance with the technological developments and computer integration, the modeling and optimization of the metal cutting processes play the major role.

Every practice regarding the machining operations in industry has relation to the theory of metal cutting since all the metal cutting operations have common mechanical principles. In this respect, the two dimensional orthogonal cutting mechanics is used to form a basis for general mechanics, and can be extended to model the geometrically complex metal removal processes such as oblique cutting. The performance of a metal cutting operation is determined by cutting parameters such as the cutting speed, feed rate, depth of cut and cutting tool geometry. For a particular metal removal process those parameters can be determined experimentally. However, empirical testing before each operation is not a practical way; therefore developing prediction models for the cutting parameters plays the key role. The main input for such a prediction model is the exerted forces during cutting operation. Depending on the tool and the cutting edge geometry, the direction of the forces changes which may increase the prediction errors higher. In addition, deformation mechanism at the third zone causes edge forces which are one of the main source of errors in cutting force predictions. Edge forces are usually determined experimentally and affected by the edge geometry of the tool, and can be relatively high when the uncut chip thickness is comparable with the hone radius. Therefore, there is a need for a method which can be used for the prediction of edge cutting forces for accurate modeling of machining processes.

In this thesis, the mechanics of orthogonal and oblique cutting is reviewed using analytical and experimental methods for different materials and process conditions. The results are used in mechanistic modeling of the cutting forces. As an important part of the experimental work, edge forces are also analyzed empirically. The effect of hone radius on the cutting process is investigated, and taken into account in force predictions using an analytical model proposed by Ozlu [20], and promising results are obtained and verified by experiments.

1.1 Literature Survey

Metal cutting is one of the oldest and most common applications in machining. Depending on the application, machining type may differ; however the basic principles remain the same. In this respect, mechanics and the dynamics of the orthogonal cutting model provide invaluable insight regarding the selection of process parameters. Merchant [1] developed a mathematical model for the orthogonal cutting process. He developed an equation for the shear angle by applying the minimum energy principle and assuming the shear zone to be a thin plane. This approach is still in use to understand the fundamentals of metal cutting. Later, Lee and Shaffer [2] and Palmer and Oxley [3] assumed a thick shear zone model and proposed shear angle prediction formulae by using laws of plasticity. In addition, Krystof [4] proposed an approach regarding the shear angle calculation based on maximum shear stress principle which assumes that the shearing occurs in the direction of maximum shear stress. Also, Oxley [3], Shaw [5] and Armarego and Brown [8] proposed analysis and prediction models for the mechanics of cutting. Although majority of the proposed models are for the orthogonal cutting process, almost all cutting processes in industry are oblique due to the geometry of industrial cutting tools and machining processes. Armarego and Brown [8], investigated the mechanics of oblique cutting in detail and presented relations between the cutting parameters such as shear angle, shear stress, friction coefficient, by extending the mechanics of orthogonal cutting. Also, Altintas [7] proposed a practical approach which can be used to predict oblique cutting forces from the orthogonal cutting tests. This method is one of accurate ways of modeling of oblique

cutting process by applying the mechanics of cutting using oblique transformations from the orthogonal data. On the other hand, Stabler [6] analyzed the oblique cutting geometry, and proposed a widely accepted chip flow law which assumes that the chip flow angle is equal to the angle of obliquity. However, this law does not consider the effect of tool geometry, friction and shear angle. Therefore, depending on the cutting conditions significant errors may be introduced in cutting force coefficient prediction.

In accordance with the technological developments, numerical and semi-analytical models have also been proposed. Altintas [7] proposed orthogonal cutting models by identifying some of the cutting parameters from cutting experiments. In recent years, numerical models using the Finite Element Method (FEM), [9] have also been used in the analysis of cutting processes. Although the FEM may provide additional predictions such as stress and temperature distribution, residual stresses etc., the computational time is usually very high. FEM method may also consider some practical aspects of the process geometry such as the edge hone radius which is the main source of edge cutting forces in the third deformation zone.

The literature indicates many attempts to understand and model the edge cutting forces. Extrapolating the machining forces to zero chip thickness using the mechanistic approach is the common way of identifying edge forces [11]. Although the accuracy of this method is reasonably high, it may yield inaccurate predictions in the out-of-calibration range. Also, as the usual case with the mechanistic approach, the insight into the physics of the flank contact can not be obtained. Another approach is the numerical modeling i.e. the FEM. Previously an FEM was developed to understand the effect of edge radius on cutting forces while considering the process variables for tool edge design optimization [12]. As a third approach, Waldorf et al. [13] proposed a slip line model for the orthogonal cutting to identify the ploughing and shearing components of the machining forces, and showed the relation between ploughing forces and hone radius experimentally. However, their results showed that the model is accurate only when chip thickness to hone radius ratio is high [13]. Later, in order to predict the stress on the tool flank, Waldorf et al. [14] utilized the ploughing characteristics of their model which requires shear flow stress and shear angle as

inputs. Waldorf et al. [14] obtained the inputs from measurements using a sharp tool, and applied classical cutting circle force equilibrium equations to determine the shear flow stress and shear angle [14]. Fang et al., on the other hand, proposed an integrated slip-line field cutting model which takes the hone radius into account and evaluates effects of several parameters on the cutting process, however without the experimental verification [15].

Former research suffers from the complexity of slip line analysis and computational effort of the FEM in the calculation of the edge cutting forces. Wu [16] developed a model for the ploughing component of the thrust force, and concluded that the penetration depth has a critical role. Then, Manjunathaiah et al. [17] extended this idea by calibrating the penetration depth based on experimental data and separated the ploughing component out of the total force. In a different study Manjunathaiah et al. [18] proposed an analytical model considering the cutting forces as a function of edge radius and shear angle explicitly. They also conducted tests in order to calibrate the shear stress of the material by proposing a new approach in material modeling. However, Manjunathaiah et al. [18] did not consider the behavior at the flank contact face. Ranganath et al. [19] proposed a similar method which takes the effective rake angle for honed tools in cutting. As can be deducted from the above review, the previous studies lack the investigation of flank contact length and the behavior of the material on the clearance face in modeling the edge forces. Also, the friction behavior of the material on the flank face has not been analyzed thoroughly. Therefore, there is a need for further research in order to represent the true behavior of the material contact at the third deformation zone.

1.2 Problem Definition

Almost every field of industry requires machining in their processes. Products are mass manufactured from a sequence of machining operations in certain amount of time and any improvement in the cycle time will reduce the total cost significantly. Therefore, modeling of the machining operations such as turning and milling is very important in terms of process effectiveness.

In the modeling of a machining operation, cutting tool and workpiece are the main factors affecting the cutting process. For instance, titanium alloys cannot be machined with the cutting parameters used for steels. The tool geometry (rake angle, clearance angle, oblique angle, etc.) and process parameters (depth of cut, cutting speed, feed rate, etc.) should be determined properly for a particular tool-workpiece couple. In this thesis, the most common workpiece materials are calibrated for different tool geometry and cutting parameters by conducting orthogonal and oblique cutting processes. Moreover, for oblique cutting, the critical parameter chip flow angle is simulated determined analytically and experimentally. Obtained results are used to predict the cutting forces which provide an insight regarding the performance of process.

The orthogonal and oblique cutting forces consist of two components, i.e. the cutting force and the edge force. Cutting forces can be predicted by mechanistic or analytical models; however, edge forces are hard to predict due to the deformation mechanism in primary and tertiary region during cutting. Moreover, the edge forces are affected by the edge hone radius, and can be relatively high when the uncut chip thickness is comparable with the hone radius. For larger hone radius it is shown that the edge becomes more resistant to chipping and helps to dampen the vibrations while cutting [14] which claims that the hone radius is very crucial for an effective machining process. Therefore, there is a need for models which can represent the true behavior of cutting process and the material when it has a contact with the hone radius. In this respect, the cutting tool edge geometry is the critical factor for edge forces in the third zone. If the cutting edge is sharp, due to the shearing mechanism the forces will occur in the primary

region and the edge cutting forces will have a minimal effect on the total machining forces. Since almost all of the practical cutting tools are honed, the forces that take place in third zone become the source of edge forces which are usually determined experimentally.

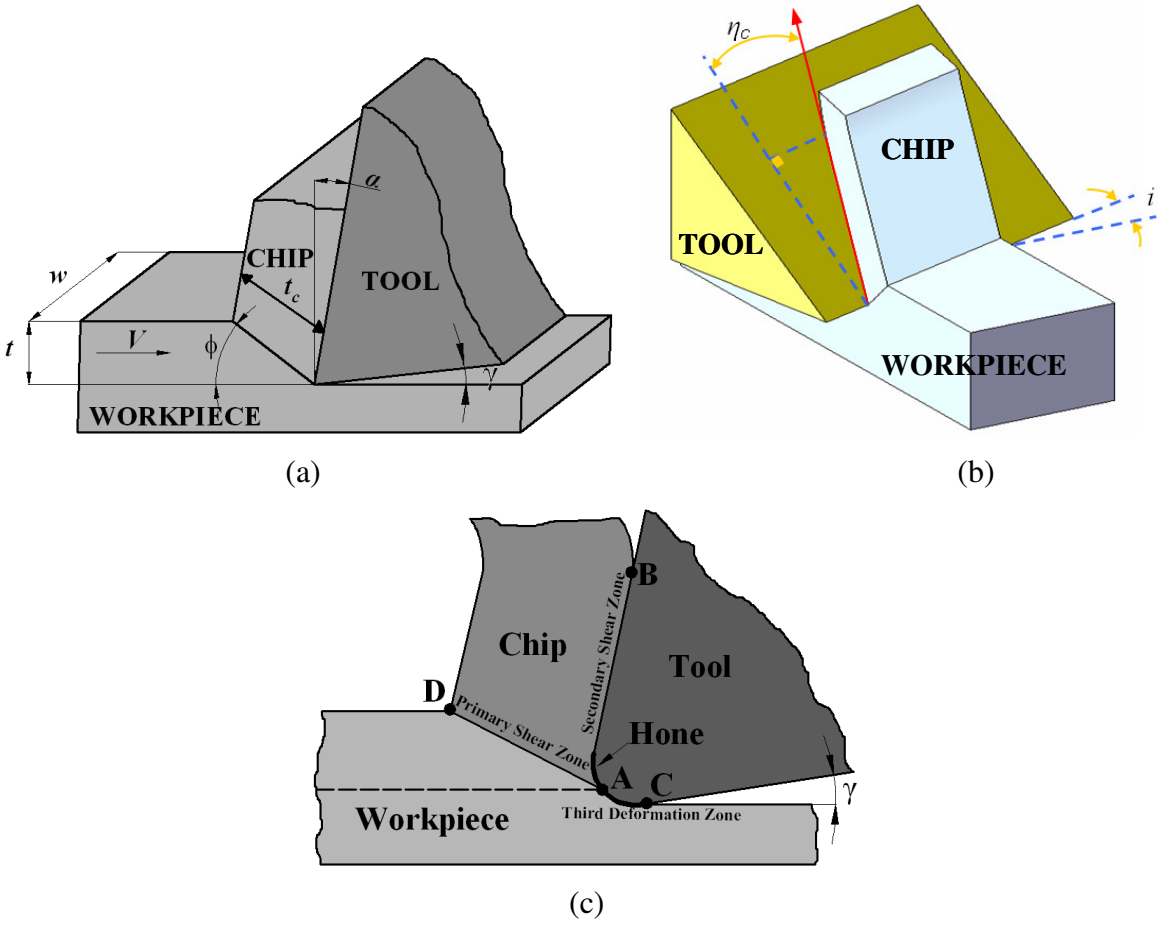

Figure 1.1: The representation of a) orthogonal cutting , b) oblique cutting and c) hone and deformation zones in orthogonal cutting [20]

In the light of these facts, the main objective of the current study is to use the proposed initial analytical model [20] for orthogonal cutting operations in order to predict the cutting forces including all the three deformation zones, and to investigate edge forces experimentally. The proposed initial analytical model [20] is compared with the FEM and experimental results. Also, detailed investigation of the effect the hone radius on the cutting mechanics is presented.

1.3 Methodology

This thesis is based on experimental analysis and investigations on the orthogonal and oblique cutting processes. In order to come up with a realistic and accurate analysis there is a need for a force model for both processes. For different and commonly used metals, AISI 4340 steels and Ti_6Al_4V alloy, calibration tests are conducted and experimental results are compared with results obtained from analytical formulations.

The fundamental parameters such as the shear angle, friction angle and shear stress are determined from the force and chip measurements. The chip thickness is measured using two different methods. In the first measurement technique, the chip thickness is measured by a micrometer, where in the second method weight measurements are used for determining the chip thickness. On the other hand, a detailed investigation on chip flow angle (see Figure 1.2) is made by applying different methods. In the first method the chip flow angle is obtained by recording the chips as it flows on the tool rake face by a video camera. As a second method, analytical prediction for the chip flow angle is conducted and finally all results are compared. Then, the cutting parameters are statistically analyzed and mechanistic model for cutting force prediction is implemented. For a certain error limit, the model is verified and continued with further analysis on the edge cutting forces.

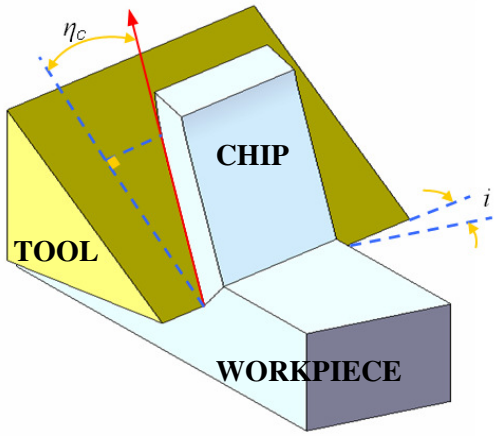

Figure 1.2: The representation of chip flow angle η_c in oblique cutting [20]

The effect of the hone radius on the cutting forces and flank contact length is investigated experimentally and analytically. An initial analytical approach for the edge cutting forces due to the third deformation zone in orthogonal cutting conditions has been proposed by Ozlu [20]. The model predicts the cutting forces by considering the normal pressure and the shear stress distributions on the edge and rake contacts in addition to the sticking and sliding friction zones on the rake face. Orthogonal cutting experiments using uncoated carbide inserts with different edge hone radii are conducted for verification and investigation purposes. The tool-material contact lengths on the flank face are measured in different test conditions, and the effects of the cutting conditions on the contact length are analyzed. The model predictions are compared by experiments and promising results are obtained.

CHAPTER 2

MECHANICS OF THE ORTHOGONAL CUTTING AND EXPERIMENTAL INVESTIGATION

In this chapter, the theory of the orthogonal cutting processes is presented together with experimental investigation using different materials. Orthogonal cutting is the simple two dimensional case of metal cutting theory and provides a crucial basis for understanding the complex geometry of general metal cutting operations. Although the orthogonal cutting geometry is relatively simple, the effect of process parameters such as feed rate, cutting speed, depth of cut etc. still needs to be investigated in order to model the complex metal cutting operations based on the orthogonal cutting. Therefore, before building prediction models, the variation of the important process parameters under a wide range of cutting conditions should be analyzed properly.

2.2 Orthogonal Cutting Mechanics

In orthogonal cutting the tool edge is perpendicular to the cutting velocity and chip flows parallel to the rake face of the tool. Since the tool orientation with respect to workpiece is perpendicular, the exerted cutting forces are in the cutting velocity and uncut chip thickness directions, called as tangential (F_t) and feed (thrust) force (F_f) respectively.

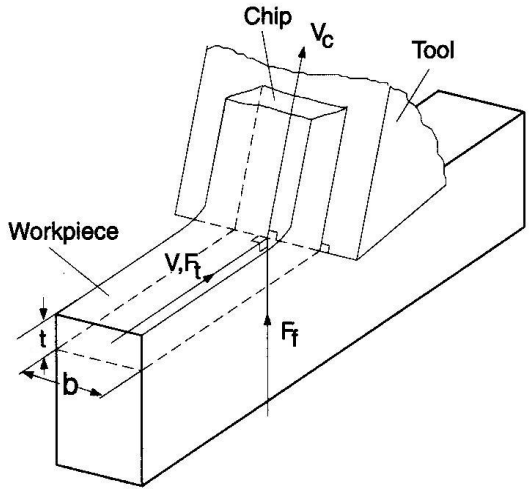

Figure 2.1: Orthogonal cutting geometry [7]

During orthogonal cutting chip formation occurs at the primary shear zone along an inclined plane at a shear angle ϕ. In the secondary deformation zone, deformed chip moves along the rake face by first sticking to the rake face, then leaves the cutting tool in the sliding region. This mechanism is investigated in the model proposed by Zorev [23]. The important parameter here is the rake angle which is the angle between tool face and a line perpendicular to the machined surface. The third deformation zone is between the flank of the tool and workpiece in which the rubbing mechanism occurs and edge forces are generated. Due to the friction mechanism between the tool and the workpiece, a contact zone is generated in both rake face and flank face [8].

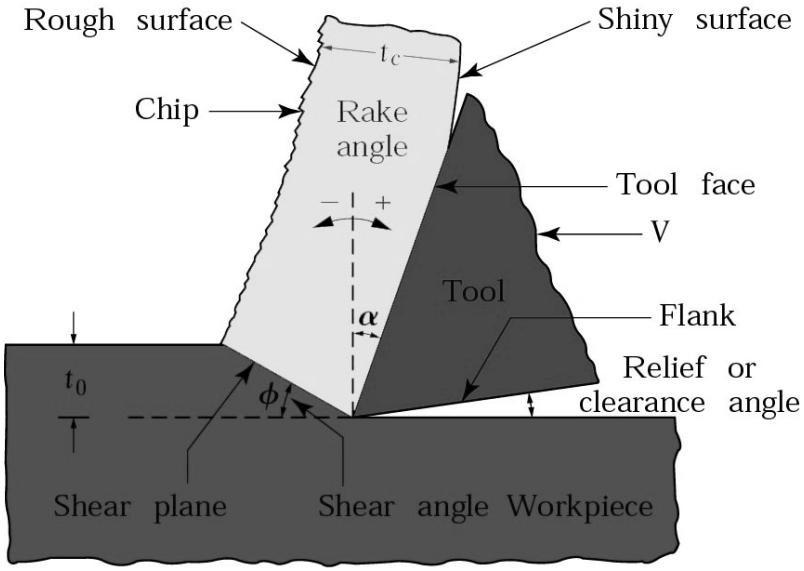

Figure 2.2: The geometrical elements of orthogonal cutting [33]

In the literature there are two types of assumptions regarding the primary shear plane analysis in orthogonal cutting. Merchant proposed an analysis by assuming a thin shear plane in primary shear zone. Then, in the light of the following assumptions Merchant developed his model [8]:

i. The tool tip is sharp and no rubbing or ploughing occurs between the tool and the workpiece
ii. The deformation is two-dimensional
iii. The stresses on the shear plane are uniformly distributed
iv. The resultant force on the chip applied at the shear plane is equal, opposite and collinear to the force applied to the chip at the tool-chip interface.

In accordance with the above conditions the following Merchants force diagram is constructed:

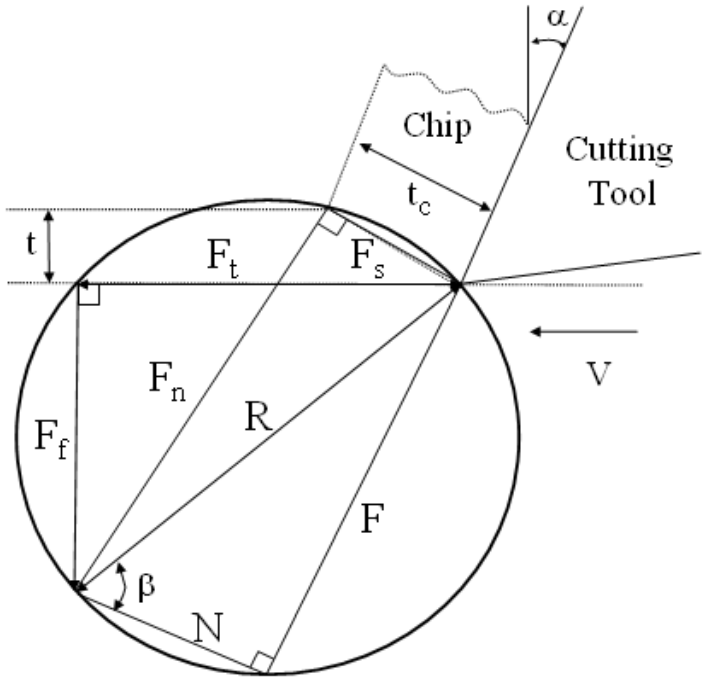

Figure 2.3: Merchant's force diagram.

According to this diagram the resultant force *R* is acting on the cutting edge has a tangential force F_t and feed force F_f components. In addition, *F* is the friction force on the rake face

and N represents the normal force on the rake face which leads to the determination of friction angle β. From the force equilibrium the resultant force R can be calculated as:

$$R = \sqrt{F_t^2 + F_f^2} \tag{2-1}$$

The tangential force is in the direction of cutting velocity, and the feed force is in the direction of uncut chip thickness. These force components are measured experimentally by using piezoelectric dynamometers mounted between the workpiece and a non-rotating part of the machine. Cutting forces are depended highly on the depth of cut, feed rate and tool geometry, which are the set of parameters determined before the cutting operation. On the other hand, shear angle and friction angle are the other crucial factors affecting the cutting forces F_t and F_f. These forces can be calculated as follows:

$$F_t = tb\left[\frac{\tau\cos(\beta-\alpha)}{\sin\phi\cos(\phi+\beta-\alpha)}\right] \tag{2-2}$$

$$F_f = tb\left[\frac{\tau\sin(\beta-\alpha)}{\sin\phi\cos(\phi+\beta-\alpha)}\right] \tag{2-3}$$

In these equations τ is the shear stress on the shear plane, ϕ is the shear angle shown in the Figure 2.2, α is the tool rake angle, t is the uncut chip thickness, b is the depth of cut and finally β is the friction angle. The main rationale in these equations is the multiplication of the sheared chip area (mm^2) with the specific cutting pressure which is called cutting force coefficients (N/mm^2).

The important thing here is the determination of shear angle, friction angle and shear stress from the orthogonal cutting tests. Shear angle can be found from the geometrical relations shown in the Figure 2.2 as a function of tool rake angle (α) and chip ratio (r_c):

$$\tan\phi = \frac{r_c\cos\alpha}{1 - r_c\sin\alpha} \tag{2-4}$$

where the chip ratio (r_c) is the ratio of uncut chip thickness over cut chip thickness

$$r_c = \frac{t}{t_c} \tag{2-5}$$

Friction angle is β can be determined by the following equation:

$$\beta = \alpha + \tan^{-1}(\frac{F_f}{F_t}) \tag{2-6}$$

In this equation α is the tool rake angle, F_f and F_t are the feed and tangential forces, respectively. It should be noted that, the force components are cutting force components and do not include the edge forces. However, the other way to determine the friction angle is by determining the coefficient of friction μ which is the ratio of friction force *F* to normal force *N* on the rake face.

$$\mu = \frac{F}{N} = \tan\beta \tag{2-7}$$

On the other hand, to calculate the shear stress τ , primary shear zone should be considered. The ratio of shear force to the shear plane area yields the shear stress.

$$\tau = \frac{F_s}{A_s} \tag{2-8}$$

The shear force acting on the shear plane and shear plane area should be derived from geometrical relations:

$$F_s = F\cos(\phi + \beta - \alpha) \tag{2-9}$$

where β is friction angle, α is tool rake angle and ϕ is the shear angle. In addition, the shear plane area is:

$$A_s = \frac{bt}{\sin\phi} \tag{2-10}$$

where *b* is the depth of cut, *t* is the uncut chip thickness and ϕ is the shear angle.

These variables can be calibrated by orthogonal cutting tests and cutting forces can be predicted mechanistically as a function of cutting parameters such as depth of cut, uncut chip thickness, tool geometry and cutting coefficients [7].

2.2 Experimental Analysis on Orthogonal Cutting

In the previous section a brief theory and the fundamentals of the orthogonal cutting process are presented. The following section is the experimental analysis of the orthogonal cutting theory for different materials, AISI 4340 steel and Ti_6Al_4V titanium alloy, under different cutting conditions. The most important outcomes of the tests are the friction angle, shear angle and shear stress are discussed thoroughly which are also needed to create the orthogonal database. These discussions will be useful in determining the dependencies of these outcomes with the cutting parameters such as rake angle, cutting speed and feed rate.

Orthogonal calibration tests for AISI 4340 steel are conducted at dry cutting conditions with TPGN 160304 P20 grade carbide inserts. The cutting speed and feed rate range is taken as 60-400 m/min and 0.1 – 0.25 mm/rev, respectively. Depth of cut is 2 mm and the average inner diameter of the workpiece was 96 mm where the average outer diameter was 100 mm.

The material and mechanical properties of the AISI 4340 steel is presented in the following Table 2.1 and the experimental results of AISI 4340 orthogonal tests are presented in appendix (Table A1). Obtained results are discussed in the following subsections.

Material Properties (Weight %)		**Mechanical Properties**
C 0.38-0.43	**Si** 0.15-0.30	**Density** (×1000 kg/m^3) 7.7-8.03
Mn 0.60-0.80	**Cr** 0.70-0.90	**Elastic Modulus** (GPa) 190-210
P 0.035 (max)	**Ni** 1.65-2.00	**Tensile Strength** (Mpa) 744.6
S 0.04 (max)	**Mo** 0.20-0.30	**Yield Strength** (Mpa) 472.3
		Hardness (Rockwell C) 24

Table 2-1: The material and mechanical properties of the AISI 4340 Steel

AISI 4340 Cutting Forces

Forces are measured by using a table type dynamometer for different cutting conditions. The following graphs represent the change of measured feed and tangential forces with respect to feed rate for different rake angles.

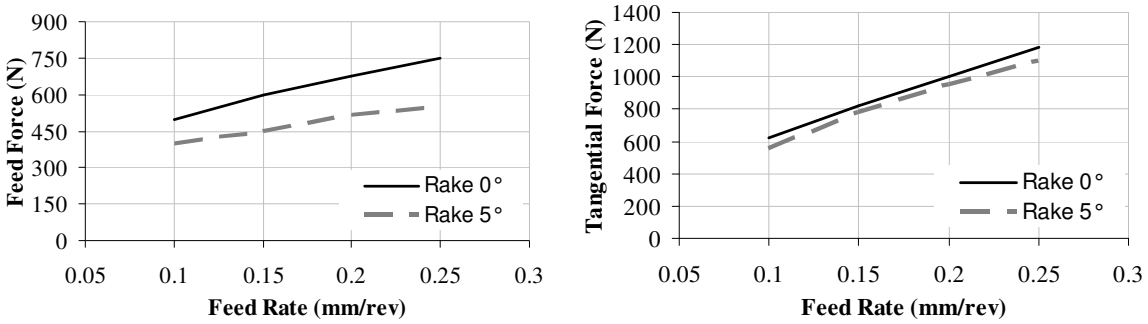

Figure 2.4: The effect of feed rate on feed force and tangential force for different rake angle and same cutting speed, V= 60 m/min.

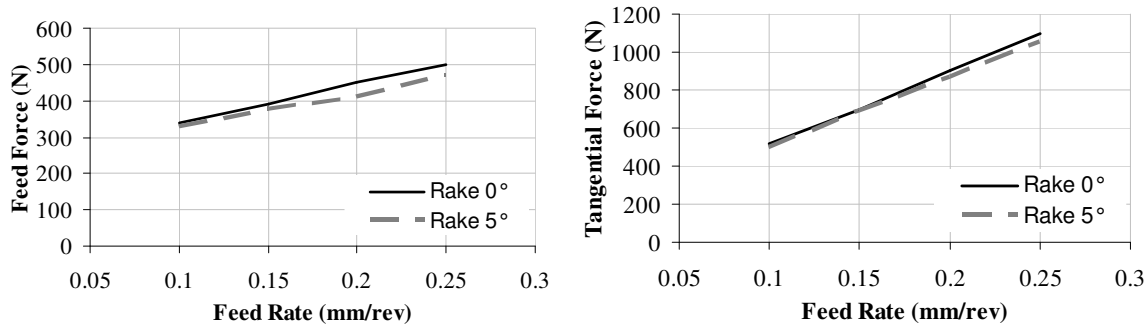

Figure 2.5: The effect of feed rate on feed force and tangential force for different rake angle and same cutting speed, V= 150 m/min.

From the Figure 2.4 and Figure 2.5 it can be observed that both force components increase with the feed rate. Also, it is seen that the forces measured with 0° rake angle are always greater than the forces measured with 5° rake. This is an expected result; from the geometrical point of view the cutting tool is more perpendicular to the cutting speed direction when the rake angle is small. Therefore, the shear strain in the primary deformation zone, which is depended on shear angle and rake angle, takes higher values at low rake angles and yields higher cutting forces. On the other hand, if the tool hone radius is comparable with the feed rate, due to rapid strain the force behavior may change in chip formation [32]. In that case rubbing may occur under the cutting edge, and affects the

measures forces. This situation is most likely to occur in low feed rates at low cutting speeds.

The other observation from the Figure 2.4 and Figure 2.5 is that the feed force and tangential force components decrease as the cutting speed increases. Figure 2.6 and Figure 2.7 show this observation for both force components. The decrease in the forces with the cutting speed can be explained by the shear strain and strain rate during cutting. The temperature increases at higher cutting speeds which decreases the yield strength of the material and increases the strain rate. When the strength of the material is decreased with temperature, shearing becomes easier and exerted forces decrease.

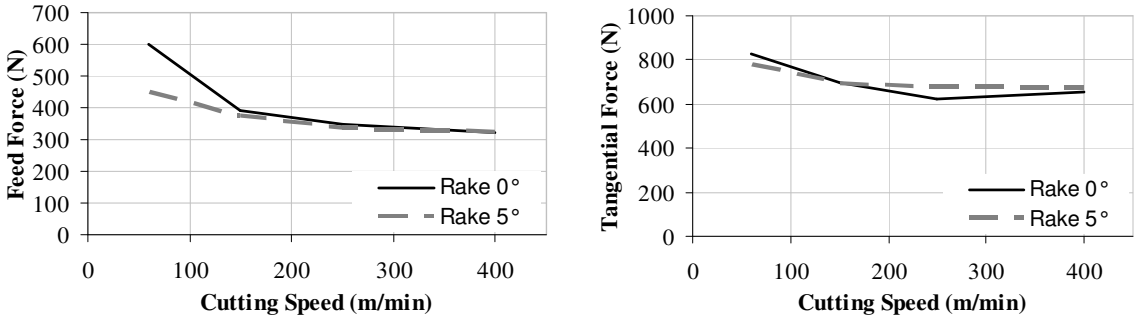

Figure 2.6: The effect of cutting speed on feed force and tangential force for different rake angle and feed rate, f= 0.15 mm/rev

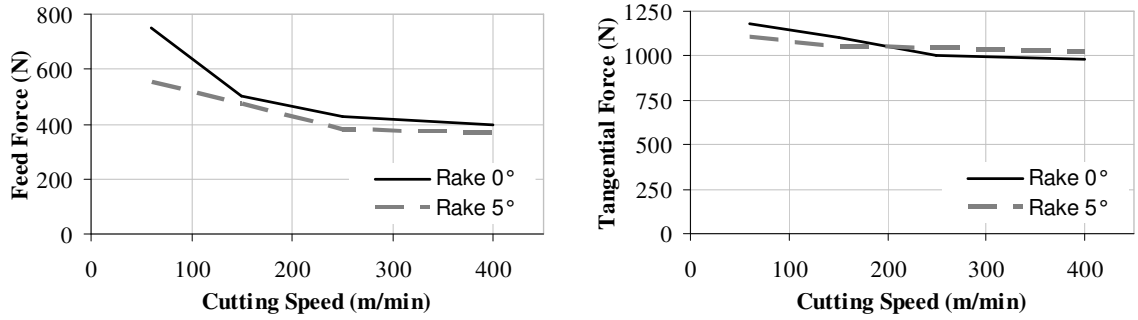

Figure2.7: The effect of cutting speed on feed force and tangential force for different rake angle and feed rate, f= 0.25 mm/rev

AISI 4340 Shear Angle :

The shear angle determines the orientation of primary shear plane during chip formation and is highly depended on chip ratio and the rake angle. As it can be seen from Figure 2.8, increasing feed rate increases the shear angle for different rake angles. The chip ratio, which is always less than 1, increases when the feed rate (uncut chip thickness) increases, therefore shear angle increases. Also, shear angle becomes higher for high rake angles. In this case, the shear plane length becomes smaller which yields smaller cutting force for a given shear stress.

From the cutting speed point of view, the trend in the shear angle is increasing and the cutting speed effect on shear angle can be explained by the cutting temperature and strain in tool-chip contact. As already explained, thermally softened metal is sheared more easily, and thus results larger shear angle.

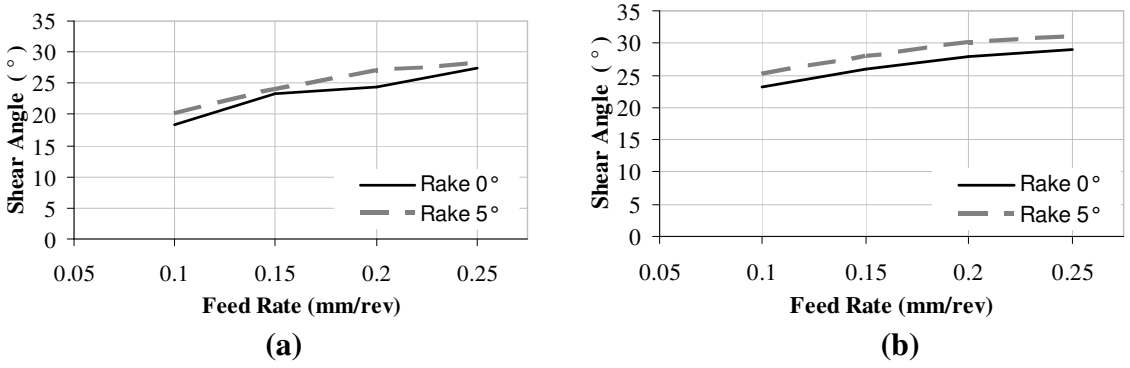

Figure 2.8: The effect of feed rate on shear angle for different cutting speeds, a) V=60 m/min b)V=150 m/min

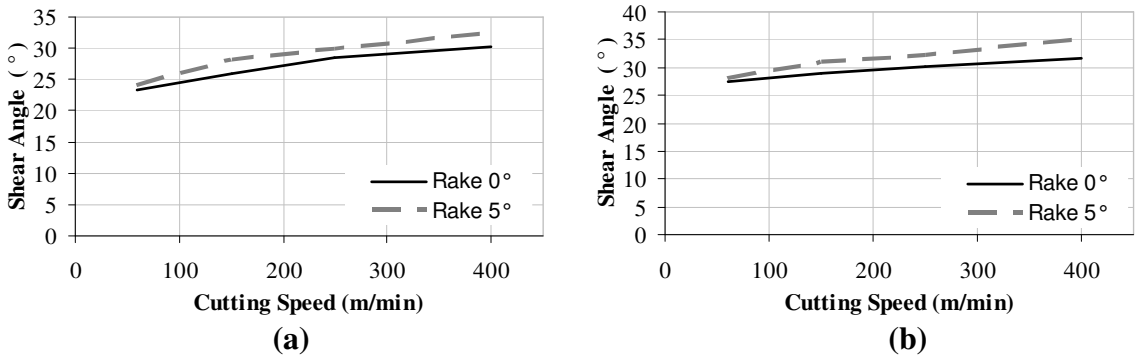

Figure 2.9: The effect of cutting speed on shear angle for different feed rates, a) f=0.15 mm/rev b) f= 0.25 mm/rev

AISI 4340 Friction Angle:

Friction angle is one of the most important varibles during cutting. It is directly related with the tool-chip contact at the rake face and has a great influence in primary deformation zone in terms of cutting temperature, build-up edge formation and tool wear. The chip contact on the rake face occurs in two regions as sticking and sliding regions [23]. In general, the friction in the sticking zone is lower than the friction in the sliding zone. As the cutting parameters change the chip behavior and friction angle change in these regions. The friction coefficient, or the friction angle, identified from the experiments is a weighted average of the friction in both zones, and referred to as the "appearent friction". The following graphs represent the variations of measured friction angle with cutting parameters such as rake angle, cutting speed, and feed rate.

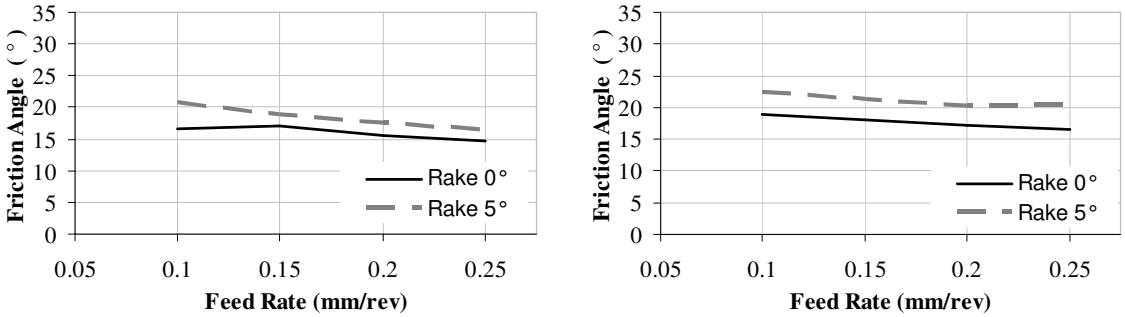

Figure 2.10 : The effect of feed rate on friction angle for different cutting speeds, a) V= 150 m/min b) V= 250 m/min

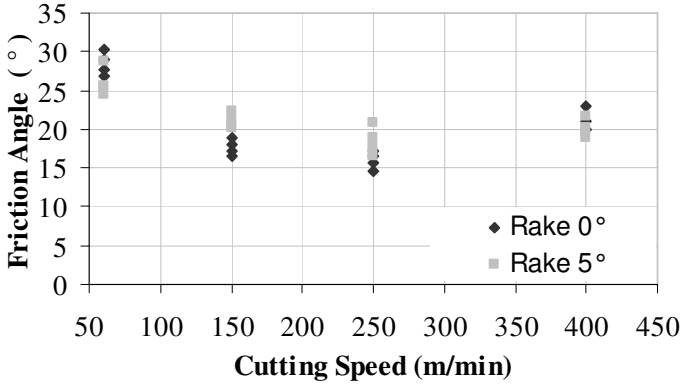

Figure 2.11: The effect of cutting speed on friction angle for different rake angles

As can be observed from Figure 2.10 and Figure 2.11 friction angle has a decreasing trend with feed rate and cutting speed. The reason of this trend can be explained by the tool-chip contact length. The tool-chip contact length is proportional to the feed rate; therefore as the feed rate increases the normal stress at the rake face increases which will increase the normal force N on the rake face as well [20]. The equation (2.7) indicates that the normal force N is inversely proportional to the coefficient of friction μ. Therefore, an increase in the normal force N decreases the coefficient of friction μ, so as the friction angle. In order to generalize the feed rate, cutting speed and rake angle effect on friction angle, it is necessary to investigate the stress distribution on the rake face.

AISI 4340 Shear Stress:

Shear stress is the other critical parameter during cutting. It affected by the tool-chip contact length on the rake face. The following graphs represent the variation in measured shear stress with the rake angle, cutting speed, and feed rate, respectively. The effect of the cutting speed, feed rate and rake angle is analyzed in Figure 2.12 and Figure 2.13. For 0° rake angle, it is observed that there is a very slight variation in shear stress. However, when the rake angle increases to 5°, the shear stress increases with the cutting speed. The primary reason for the increase is the strain rate and tool-chip contact which are also affected by the rake angle as well. In order to understand the rake angle effects on the shear stress, the strain rate sensitivity for the material should be investigated for different rake angles [18].

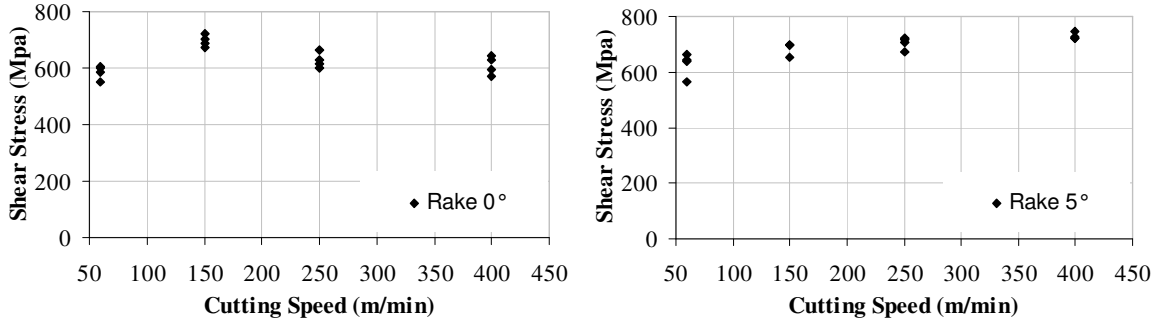

Figure 2.12 : The effect of cutting speed on shear stress for different rake angles

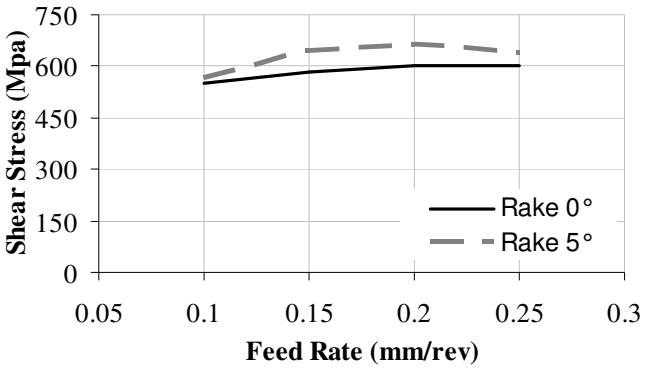

Figure 2.13: The effect of feed rate on shear stress for different rake angles

Figure 2.13 shows the feed rate and rake angle effect on the shear stress. It is observed that shear stress remains constant except for the lowest feed rate. There is a slight increase in shear stress when the feed rate increases from 0.1 mm/rev to 0.15 mm/rev. This side observation can be explained by the friction behavior for the lowest feed rate. Shear force may be increased due to tool-chip contact length and friction in a small size deformation zone and increased the shear stress. However the increase in the shear stress with feed rate cannot be generalized for every material.

Orthogonal Database for AISI 4340 Steel:

A series of orthogonal cutting tests are conducted on AISI 4340 steel. Fundamental parameters, such as shear stress, friction angle and shear angle, are identified from orthogonal cutting tests (see Appendix Table A-1) and their relations with cutting parameters are statistically analyzed to model the cutting forces mechanistically. In the following section, derived equations for the orthogonal database for AISI 4340 steel are presented. The notations and units are as follows:

Rake angle: α (°)

Friction angle: β (°)

Shear angle: ϕ (°)

Uncut chip thickness : t (mm/rev)

Shear stress: τ_s (MPa)

The error between the fitted equations and experimental results are calculated as follows:

$$error = \frac{x_{\exp} - x_{eqn}}{x_{\exp}} \times 100 \tag{2-11}$$

The average absolute error is calculated by summing up the absolute value of the error and dividing to the number of the data. The following table represents the statistical relation regarding the fundamental parameters in AISI 4340 orthogonal tests.

Parameter	Equation
Friction Angle	$\beta = 20.6 + 0.12\alpha$
Shear Angle	$\phi = \tan^{-1}\left(\frac{r_c \cos(\alpha)}{1 - r_c \sin(\alpha)}\right)$ $r_c = C_0 h^{C_1}$ $C_0 = 0.8477 - 0.0048\alpha$ $C_1 = 0.2775 - 0.0047\alpha$
Shear Stress	$\tau_s = 650$

Table 2-2: Orthogonal database for AISI 4340 steel

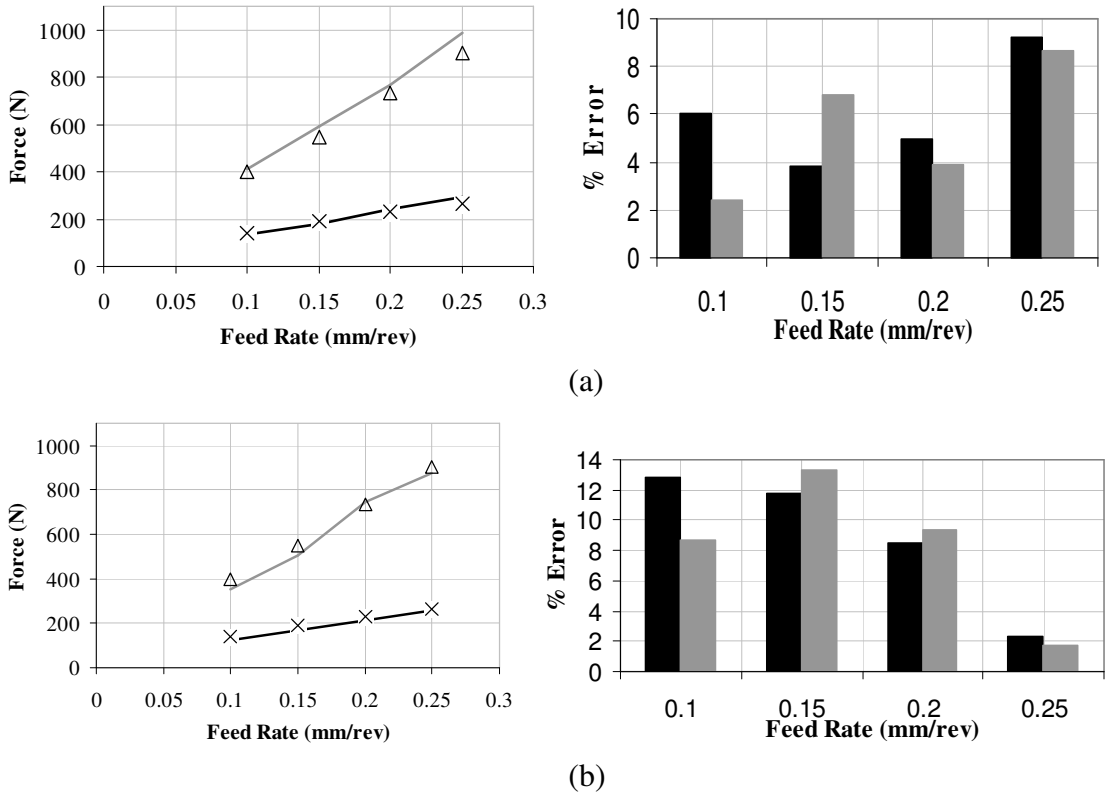

Figure 2.14: The comparison of measured feed (black) and tangential (grey) cutting forces with experimental results (markers) and percentage errors between mechanistic model and experiments for AISI 4340 steel with carbide tool having 0º rake angle at cutting speeds of (a) 150 m/min, (b) 250 m/min

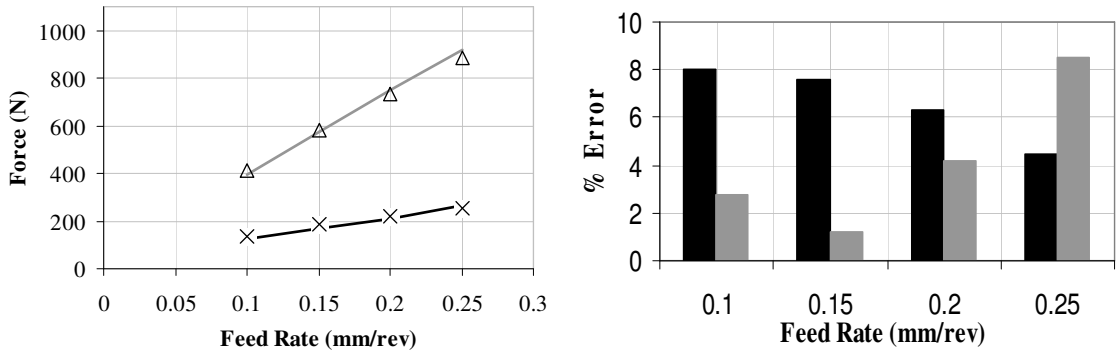

(a)

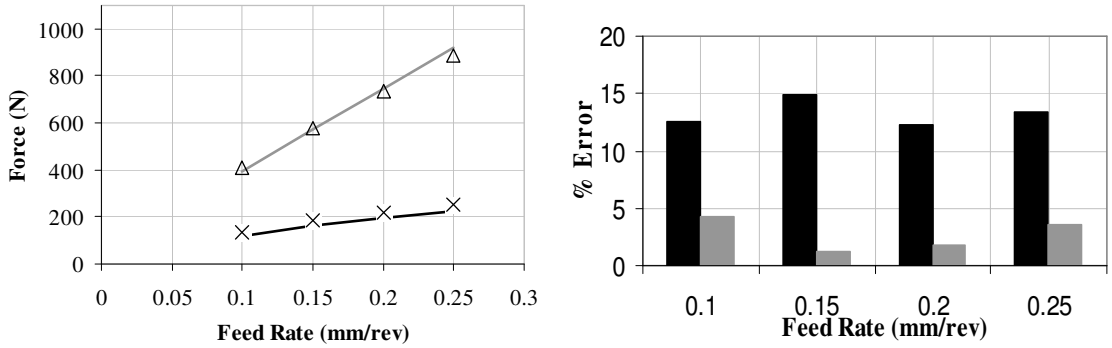

(b)

Figure 2.15: The comparison of measured feed (black) and tangential (grey) cutting forces with experimental results (markers) and percentage errors between mechanistic model and experiments for AISI 4340 steel with carbide tool having 5º rake angle at cutting speeds of (a) 150 m/min, (b) 250 m/min

From the force prediction results in Figure 2.15, it can be deduced that experiments are consistent with the prediction results. The average error is 10 % and 8 % for feed force and tangential force predictions.

For Ti_6Al_4V titanium alloy, calibration tests are conducted and forces are mechanistically modeled for various cutting conditions. Ti_6Al_4V orthogonal tests are conducted at dry conditions with 3-10 m/min speed range and 0.06 – 0.18 mm/rev feed rate range. The average inner diameter of the workpiece was 97.4 mm where the average outer diameter was 101.7 mm at the axial location on the part. Also, HSS sharp cutting tools with different geometrical properties are used in Ti_6Al_4V orthogonal cutting tests. Experimental investigation of Ti_6Al_4V is conducted with tool having two different clearance angles and seven different rake angles at different feeds and cutting speeds. The raw data is presented in appendix Table A-2 and Table A-3.

Ti_6Al_4V Alloy Cutting Forces:

The following figures represent the cutting forces in Ti_6Al_4V orthogonal cutting tests for different rake angle and cutting speeds. The trend is the same as AISI 4340 cutting force values.

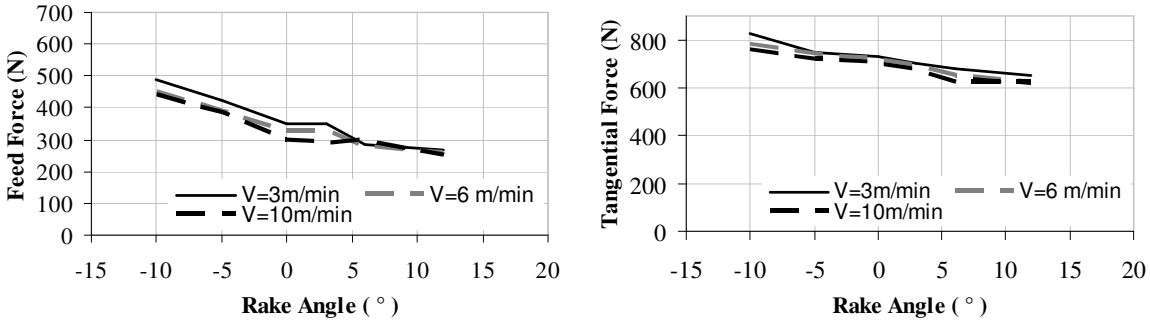

Figure 2.16: Change in the Ti_6Al_4V cutting forces with rake angle for same feed rate and clearance angle 5° , f=0.12 mm/rev.

As can be observed from Figure 2.16, both feed and tangential cutting forces decrease with the increasing rake angle and cutting speed in Ti_6Al_4V orthogonal tests due to the strain effect. The following equation (2.12) explains the relation between average strain and rake angle.

$$\dot{\gamma}_{av} = \frac{V\cos\alpha}{t\cos(\phi-\alpha)} \tag{2-12}$$

In this equation, V stands for cutting speed, α rake angle, t uncut chip thickness and ϕ shear angle. The following Figure 2.17 shows the change in the strain with rake angle for same cutting speed and feed rate.

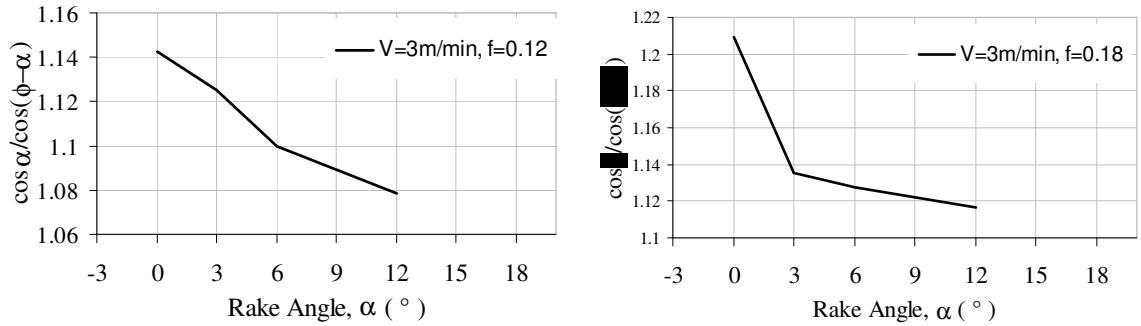

Figure 2.17 : Change in the strain with the rake angle for constant cutting speed and feed rate.

As can be observed from Figure 2.17, in Ti_6Al_4V orthogonal cutting tests, increasing rake angle decreases the strain. Also, along with the temperature increase material is thermally softened and shearing occurs easily. This is the reason why the cutting forces are decreasing with increasing rake angle for AISI 4340 steel and Ti_6Al_4V alloy. However, depending on the material behavior under high cutting speeds this implication can not be generalized for every material.

Ti_6Al_4V Alloy Shear Angle:

Shear angle variation is analyzed for different conditions in Ti_6Al_4V orthogonal cutting tests. The following figures show the effect of rake angle and cutting speed on shear angle. Since the shear angle is highly depended on rake angle, the variation is much higher. Increasing rake angle increases shear angle. Also, in Figure 2.16 it is shown that the forces are decreasing with increasing rake angle; therefore it can be concluded that higher shear angle yields lower cutting forces for the same cutting speed.

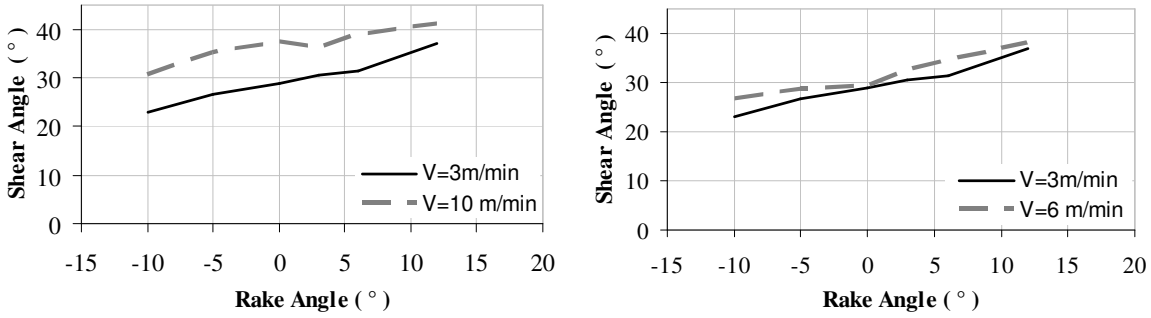

Figure 2.18 : The effect of rake angle on Ti_6Al_4V shear angle for different cutting speeds

Figure 2.19 shows that the shear angle increases as the feed rate increases for the same cutting speed. This is an expected result due to the increased chip ratio with increasing feed rate.

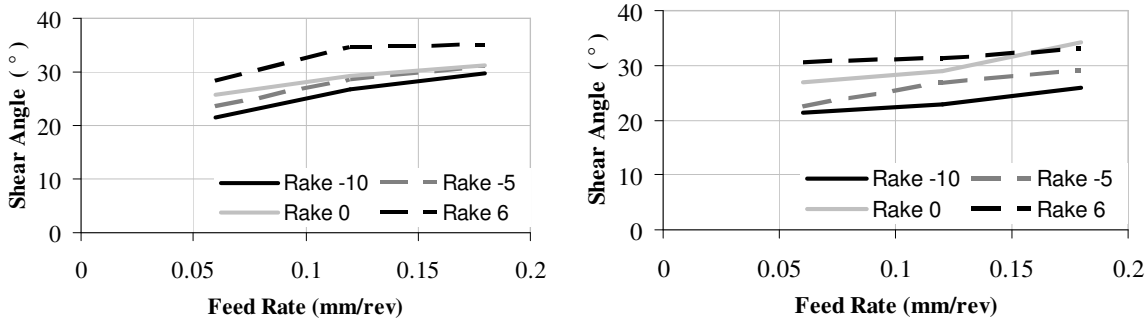

Figure 2.19 : Feed rate effect on Ti_6Al_4V shear angle for different rake angles

Ti_6Al_4V Alloy Friction Angle:

The friction angle is directly related to the coefficient of friction between the tool and chip on the rake face (see equation 2-7). Therefore, depending on the material properties the interaction between tool and chip may vary during cutting. In this respect, Ozlu [20] investigated the apparent coefficient of friction for different materials and came up with the following results.

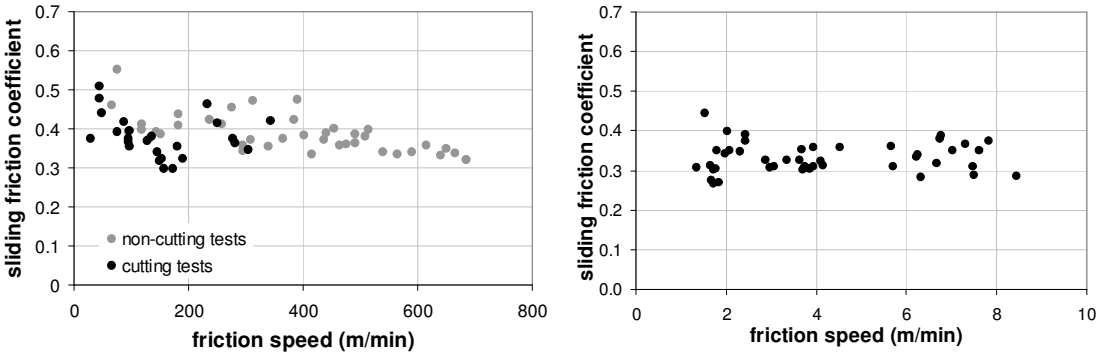

(a) (b)

Figure 2.20: Sliding friction coefficients between (a) AISI 4340 steel and uncoated carbide tool and (b) Ti6Al4V alloy with HSS cutting tool with varying friction speeds. [20]

According to this study, the coefficient of friction in AISI 4340 steel tests decreases from 0.55 to 0.35 as the friction speed increases. However, in Ti_6Al_4V orthogonal tests, the coefficient of friction remained the same as the speed increases. Ozlu [20] attributes this situation to the different hardness values of materials. The hardness of AISI 4340 is 24 Rockwell C where Ti_6Al_4V is 36 Rockwell C. These findings are consistent with our case,

which yields almost constant friction angle with increasing cutting speed for the same feed rate.

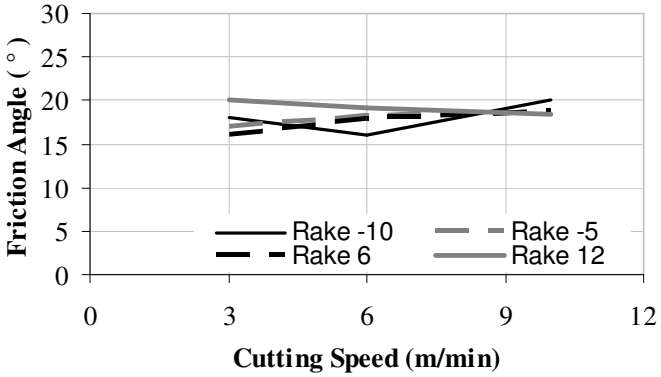

Figure 2.21: Cutting speed effect on Ti_6Al_4V friction angle for different rake angles

On the other hand, change in the friction angle with the rake angle is also observed in Ti_6Al_4V calibration tests. The results in Figure 2.22 showed that friction angle has a decreasing trend with rake angle for the same feed rate. However, this is not the general trend for the friction angle. Usually, friction angle increases with the rake angle due to the increase in tool-chip contact length. The reason of this side observation can be low cutting speeds in cutting tests. This could be one explanation for decreasing friction angle with rake angle. Although the decrease in the friction angle is not too much, there is a need for further research on the behavior of friction angle with increasing rake angle.

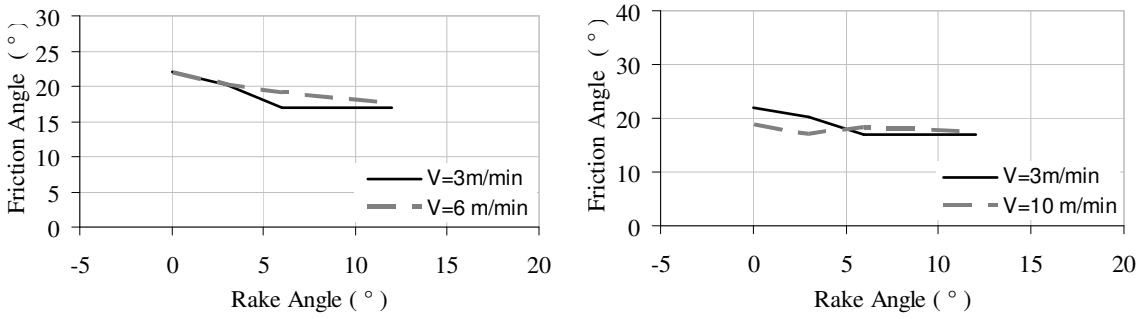

Figure 2.22: Rake angle effect on Ti_6Al_4V friction angle for different cutting speeds

Ti_6Al_4V Alloy Shear Stress:

The behavior of shear stress in Ti_6Al_4V orthogonal cutting tests is important to create the orthogonal database. Figure 2.23 anf Figure 2.24 show the effect of cutting speed , rake angle and feed rate on shear stress.

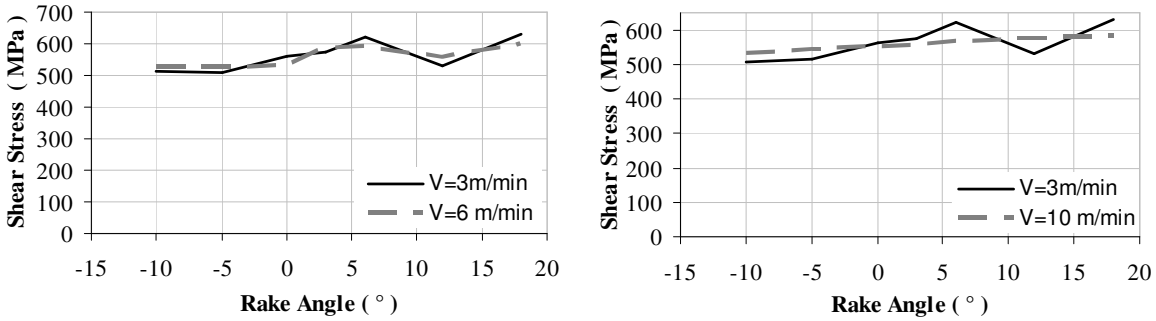

Figure 2.23: Rake angle effect on Ti_6Al_4V shear stress for different cutting speeds

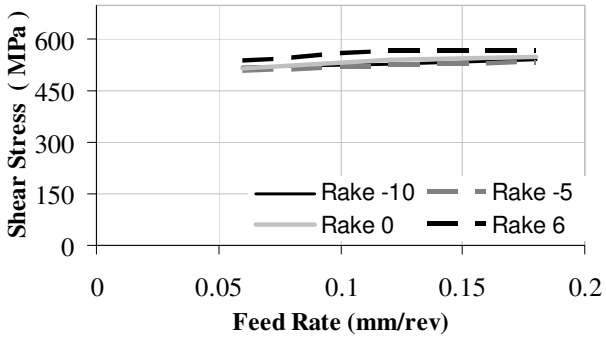

Figure 2.24: Feed rate effect on Ti_6Al_4V shear stress for different rake angles

As it is observed from the Figure 2.24, shear stress values do not significantly change with the increasing rake angle, cutting speed and feed rate. Supporting this observation, the average shear stress reflects the general behavior of shear stress under different cutting conditions.

Orthogonal Database for Ti_6Al_4V Alloy:

A series of orthogonal cutting tests are conducted on Ti_6Al_4V alloy. However, demonstrating every possible cutting condition is impratical due to time and money constraints. Therefore, the fundamental parameters, such as shear stress, friction angle and shear angle, are identified from orthogonal cutting tests (see Appendix Table A-3) and their relations with cutting parameters are statistically analyzed to model the cutting forces mechanistically. In the following section, derived equations for the orthogonal database for Ti_6Al_4V alloy are presented. The notations and units are as follows:

Rake angle: α (°)

Friction angle: β (°)

Shear angle: ϕ (°)

Uncut chip thickness: t (mm/rev)

Shear stress: τ_s (MPa)

The error between the fitted equations and experimental results are calculated as follows:

$$error = \frac{x_{\exp} - x_{eqn}}{x_{\exp}} \times 100 \tag{2-13}$$

The average absolute error is calculated by summing up the absolute value of the error and dividing to the number of the data. The following table represents the statistical relation regarding the fundamental parameters in Ti_6Al_4V alloy orthogonal tests.

Parameter	**Equation**
Friction Angle	$\beta = 19.95$
Shear Angle	$\phi = \tan^{-1}\left(\frac{r_c \cos(\alpha)}{1 - r_c \sin(\alpha)}\right)$ $r_c = C_0 h^{C_1}$ $C_0 = 0.9579 + 0.0051\alpha$ $C_1 = 0.2295 - 0.0041\alpha$
Shear Stress	$\tau_s = 525$
Tangential edge cutting force coefficient	$K_{te} = 50$ (Clearance 5º)
Feed edge cutting force coefficient	$K_{fe} = 73$ (Clearance 5º)

Table 2-3: Orthogonal database for Ti_6Al_4V titanium alloy for cutting tool with clearance angle 5º

The cutting forces are calculated according to Table 2.3 and compared with the experimental results. A total of 36 cutting tests with tool having rake angles of 0º, 3º, 6º, and 12º and a clearance angle of 5º are compared in the figures below. According to the obtained results, the percentage error between the measured forces and the calculated forces are much higher in low cutting speeds and high feed rates. Considering the average percentage errors, the agreement between the experiments and mechanistic model is found to be reasonable.

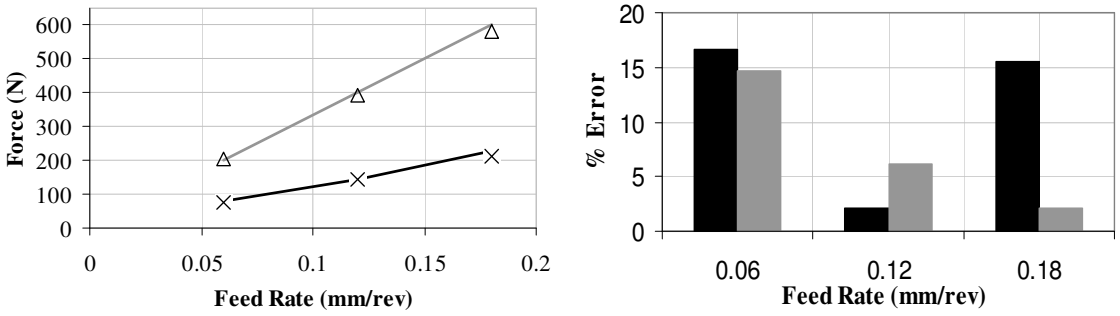

(a)

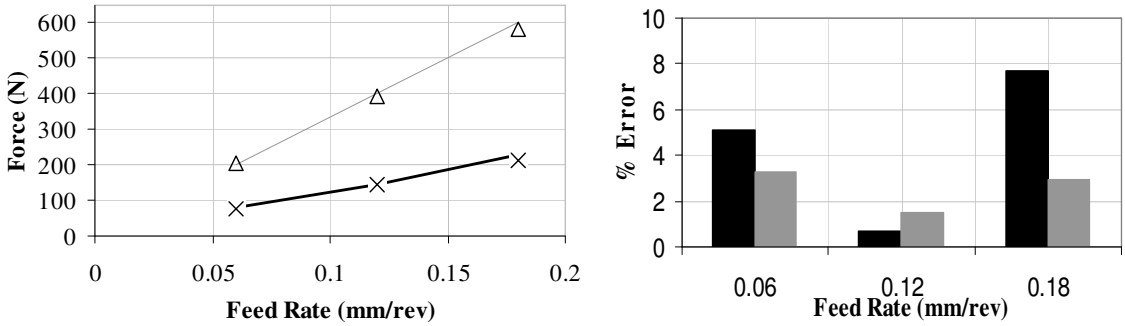

(b)

Figure 2.25: The comparison of measured feed (black) and tangential (grey) cutting forces with experimental results (markers) and percentage errors between mechanistic model and experiments for Ti_6Al_4V alloy with HSS tool having 5º clearance angle and 12º rake angle at cutting speeds of (a) 3m/min, (b) 10 m/min

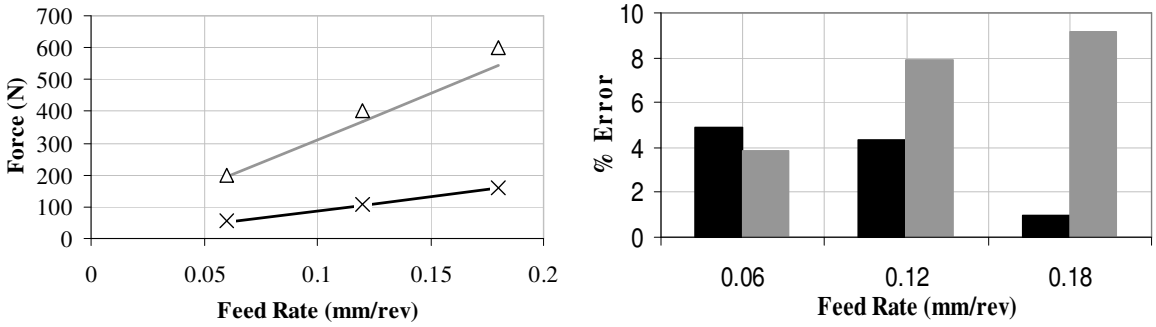

(a)

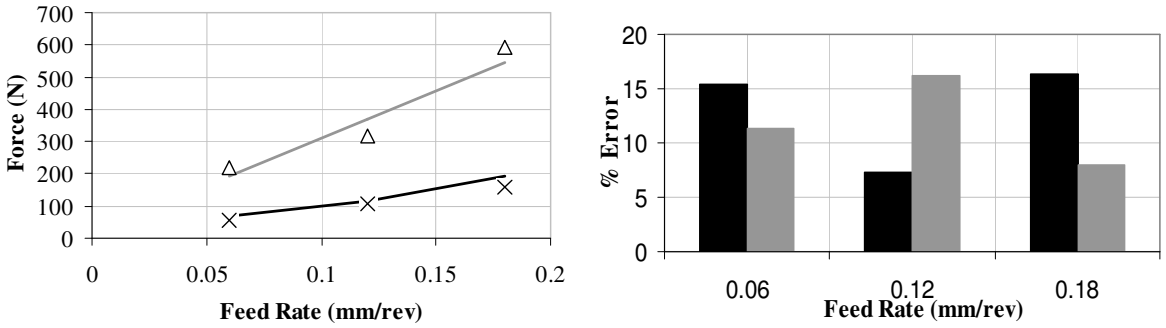

(b)

Figure 2.26: The comparison of measured feed (black) and tangential (grey) cutting forces with experimental results (markers) and percentage errors between mechanistic model and experiments for Ti_6Al_4V alloy with HSS tool having 5° clearance angle and 12° rake angle at cutting speeds of (a) 3m/min, (b) 10 m/min

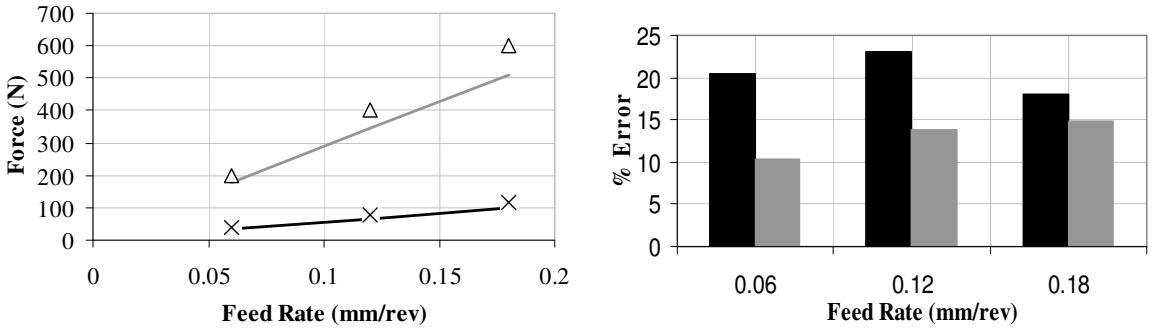

(a)

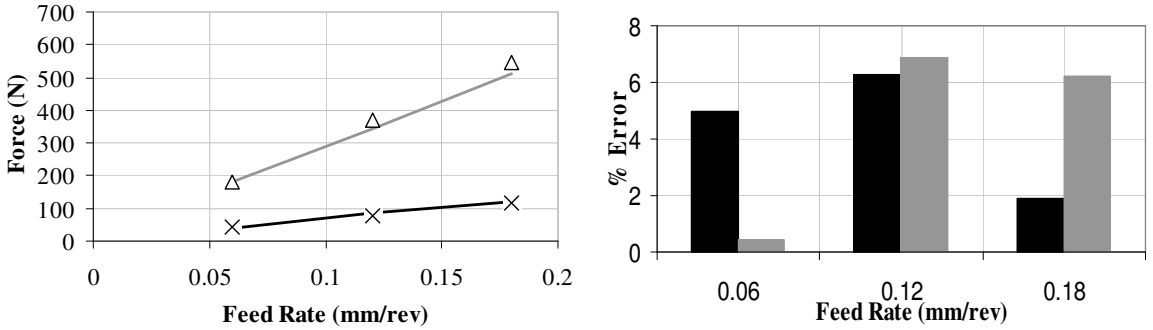

(b)

Figure 2.27: The comparison of measured feed (black) and tangential (grey) cutting forces with experimental results (markers) and percentage errors between mechanistic model and experiments for Ti_6Al_4V alloy with HSS tool having 5° clearance angle and 12° rake angle at cutting speeds of (a) 3m/min, (b) 10 m/min

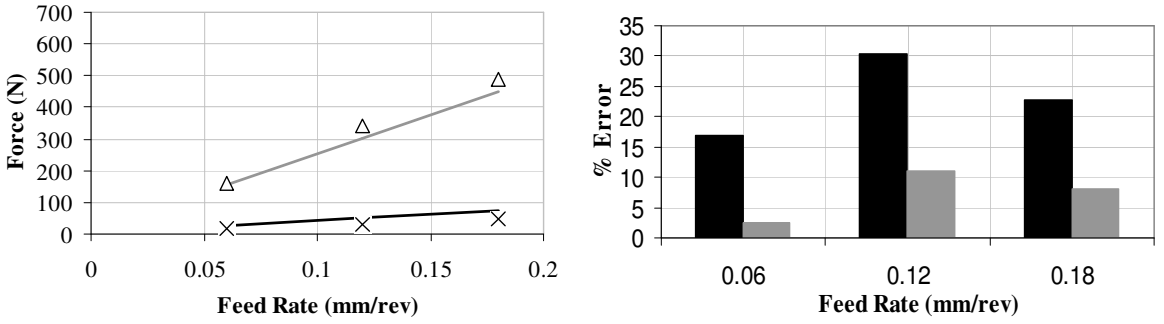

(a)

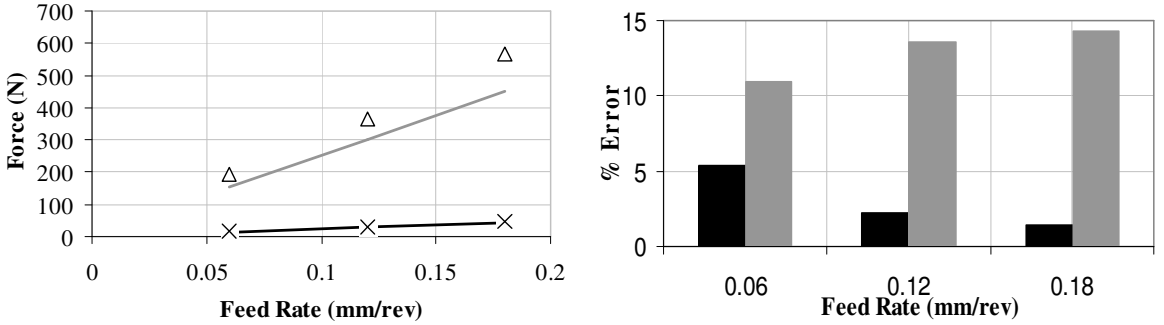

(b)

Figure 2.28: The comparison of measured feed (black) and tangential (grey) cutting forces with experimental results (markers) and percentage errors between mechanistic model and experiments for Ti_6Al_4V alloy with HSS tool having 5° clearance angle and 12° rake angle at cutting speeds of (a) 3m/min, (b) 10 m/min

To sum up, in this chapter the orthogonal cutting experiments and mechanistic force predictions are applied for AISI 4340 steel and Ti_6Al_4V titanium alloy under different cutting conditions. The followings are the general observations regarding the behavior of two metals in terms of important cutting parameters :

- Shear stress takes almost constant values with increasing feed rate and cutting speed for both AISI 4340 steel and Ti_6Al_4V alloy. Also, a slight increase (5% on the average) with the rake angle is observed. Normally, shear stress is expected to have a decreasing trend with increasing rake angle due to reduced pressure on the shear plane. This increasing trend could stem from the cutting conditions.
- Friction angle shows different trend for AISI 4340 steel and Ti_6Al_4V alloy with rake angle. In Ti_6Al_4V orthogonal tests, it is observed that friction angle has a decreasing trend with rake angle. This is not an expected result, however tests are conducted at low cutting speeds (3 m/min, 6 m/min and 10 m/min) with a sharp cutting tool. At

low cutting speeds, the contact is in sticking condition and therefore the effect of the sliding zone is minimal. Normally increasing rake angle would result in lower pressure on the rake, and thus longer sliding zone which is not observed in these low cutting speeds.

- Shear angle has the same trend for both materials and is increasing with the feed rate and rake angle. This is due to the reduced pressure on the shear plane at higher rake angles.

CHAPTER 3

MECHANICS OF THE OBLIQUE CUTTING AND EXPERIMENTAL INVESTIGATION

In this chapter, the theory of the oblique cutting processes is presented together with experimental investigation for Ti_6Al_4V titanium alloy. The main difference between the orthogonal cutting and oblique cutting stems from the tool inclination (oblique) angle. The existence of inclination angle makes the cut chips move on the rake face with a chip flow angle η and creates the force in third direction (radial force) which increases the complexity of cutting process. However, almost all machining processes in industry are oblique; therefore it is very important to investigate the mechanics of oblique cutting process in terms of important process parameters such as shear angle, friction angle, shear stress, chip flow angle etc.

3.1 Oblique Cutting Mechanics

As it is mentioned in Chapter 2, the mechanics of the more complex cutting processes can be modeled based on the orthogonal cutting. Based on this assumption, oblique cutting and orthogonal cutting tests are conducted for the same cutting conditions and material. Then, the orthogonal cutting tests are transformed to oblique cutting by transformation formulae proposed by Altintas [7] to test whether the transformation results are consistent with the experimental oblique cutting tests. Also, the variation of the process parameters are investigated for different conditions and chip flow angle is determined by various methods. In the first method the chip flow angle is obtained by recording the chips as it flows on the tool rake face by a video camera. As a second method, analytical

prediction for the chip flow angle is conducted and finally all results are compared. The following Figure 3.1 represents the geometry of oblique cutting and direction of forces with chip flow angle.

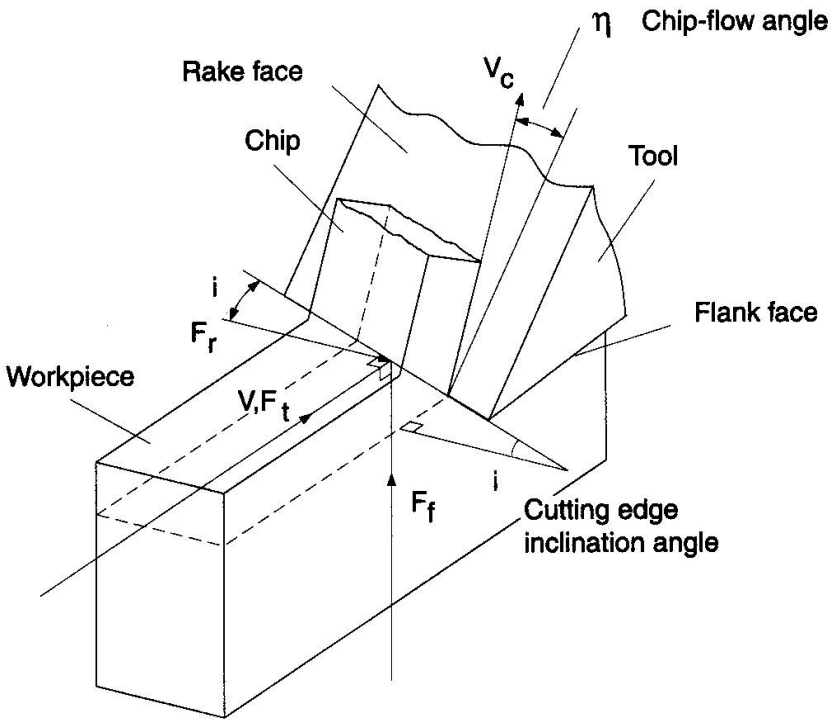

Figure 3.1: Oblique cutting geometry

Investigations regarding the oblique cutting mechanism have been studied over years and various approaches have been developed. Altintas [7] describes the geometry of the oblique cutting in the Figure 3.2 below, and introduces the normal plane, shear plane, rake face and cutting edge. In oblique cutting, due to the existence of oblique angle *i* forces are exerted in *x, y,* and *z* directions. Analysis on oblique cutting processes assumes that if the all force and velocity vectors are projected on the normal plane the cutting parameters of the oblique cutting will be equivalent to the orthogonal cutting [7]. This assumption provides a solution of complex oblique cutting parameters based on orthogonal cutting parameters. The accuracy of this assumption can be verified by conducting experimental analysis on orthogonal and oblique cutting tests.

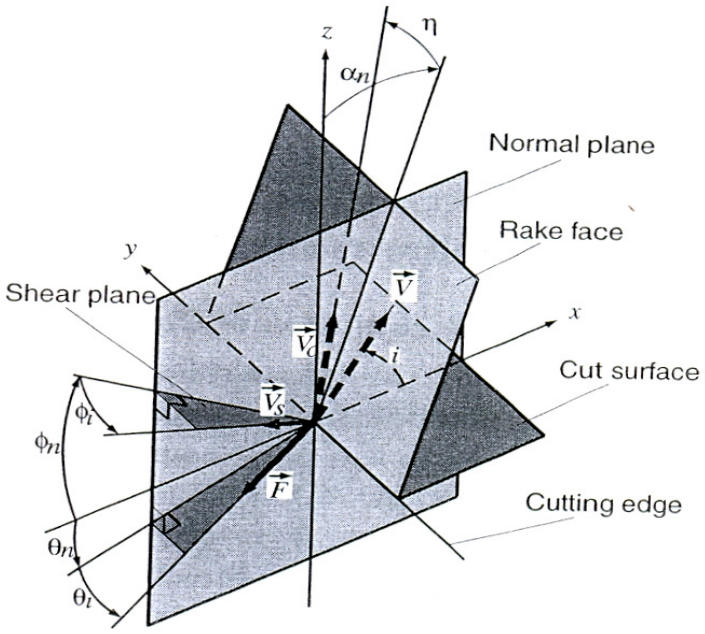

Figure 3.2: The geometry of oblique cutting with velocity and force vectors [7]

The existence of oblique angle leads several definitions on the tool rake angle and shear angle. The normal rake angle (α_n) is measured in a normal plane to the cutting edge, the velocity rake (α_v) is the angle measured in the plane parallel to the cutting velocity vector ($\vec{V}$) and perpendicular to the cut surface and finally the effective rake angle (α_e) is measured in the cutting velocity vector ($\vec{V}$) and chip flow velocity vector ($\vec{V}_c$) plane. Same definitions are valid for the normal (ϕ_n) and effective shear angle (ϕ_e). However, according to the assumptions described above, the angles in the normal plane are used in the experimental analysis. [25].

In the oblique cutting model, force and stress relationships are different than the orthogonal cutting. The resultant force *R* is not perpendicular to the machined surface as in the orthogonal cutting and chip is not moving straight on the rake face which are important for force derivations. In order to determine the three force components in oblique cutting some assumptions are made as in the orthogonal cutting. These assumptions are [8]:

i. The tool tip is sharp and no ploughing forces act on the tool tip

ii. The stress distribution on the shear plane is uniform

iii. The resultant force *R* acting on the chip at the shear plane is equal, opposite and collinear to the force acting on the chip at rake face.

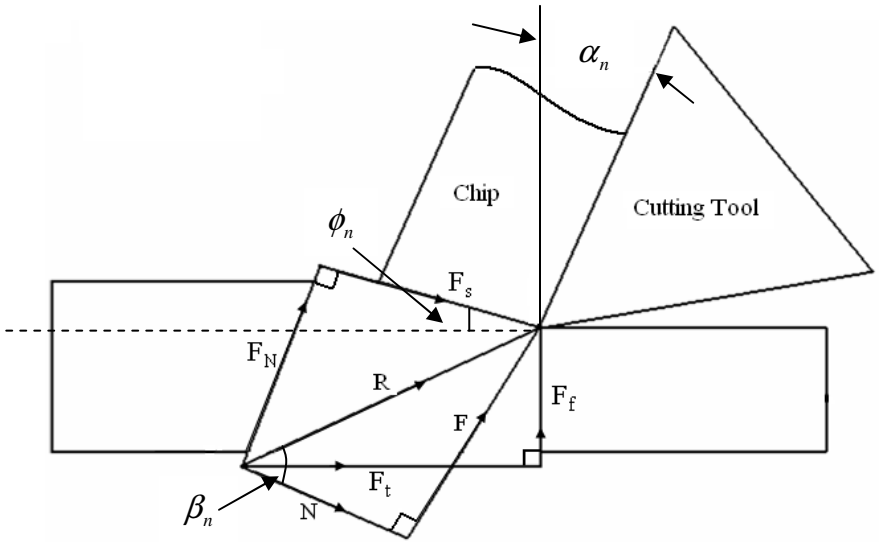

Figure 3.3 The oblique cutting forces

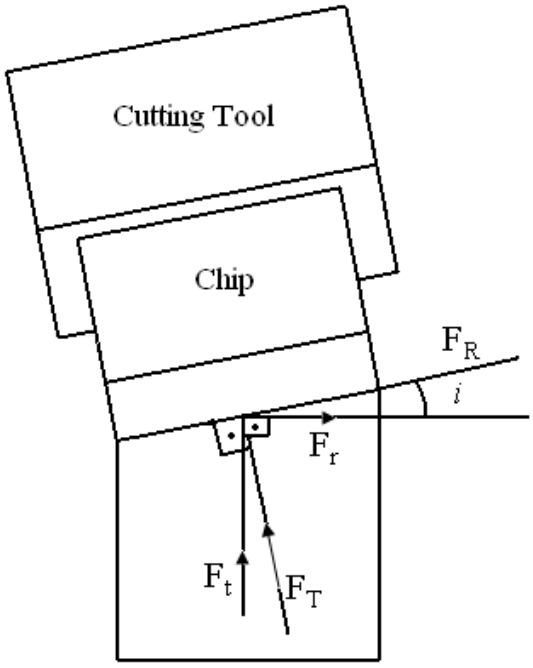

Figure 3.4 The radial force component in oblique cutting

The figure above represents the force components in oblique cutting. According to this Figure 3.3 the resultant force has two components in two planes. On the shear plane shear force (F_S) is acting where on the rake face the friction force (*F*) and normal force (*N*) components determine the resultant force.

$$R = \sqrt{F_t^2 + F_f^2 + F_r^2} \tag{3-1}$$

From this figure the individual cutting force components can be determined as:

$$\begin{aligned} F_t &= K_{tc} bt \\ F_f &= K_{fc} bt \\ F_r &= K_{rc} bt \end{aligned} \tag{3-2}$$

where *b* is the depth of cut, *t* is the uncut chip thickness and K_{tc}, K_{fc} and K_{rc} are the cutting force coefficients as a function of shear stress (τ), normal rake angle (α_n), oblique angle (*i*), normal shear angle (ϕ_n), normal friction angle (β_n) and chip flow angle (η). From the geometrical relations in oblique cutting (Figures 3.3 and Figure 3.4) the explicit form of the cutting force components can be derived.

The direction of the shear force can be found by

$$\tan F_S^{'} = \frac{F_R}{F_S} = \frac{F \tan \eta}{R \cos(\phi_n + \beta_n - \alpha_n)} \tag{3-3}$$

where the ratio of $\frac{F}{R}$ is simply $\sin \beta_n$, therefore the shear force direction turns out to be

$$\tan F_S^{'} = \frac{F_R}{F_S} = \frac{\tan \eta \sin \beta_n}{\cos(\phi_n + \beta_n - \alpha_n)} \tag{3-4}$$

On the other hand, the shear force is can be defined as,

$$F_S = \tau A_S = \tau \frac{bt}{\sin \phi_n \cos i} \tag{3-5}$$

From Figure 3.4, the tangential force F_t, can be written as

$$\begin{aligned} F_t &= F_T \cos i + F_R \sin i \\ F_t &= F_S \frac{\cos(\beta_n - \alpha_n)\cos i}{\cos(\phi_n + \beta_n - \alpha_n)} + F_S \sin F_S^{'} \sin i \end{aligned} \tag{3-6}$$

By plugging the equation 3-5 into equation 3-6, tangential force component can be found as:

$$F_t = tb\left[\frac{\tau}{\sin\phi_n}\frac{\cos(\beta_n - \alpha_n) + \tan i \tan\eta \sin\beta_n}{\sqrt{\cos^2(\phi_n + \beta_n - \alpha_n) + \tan^2\eta \sin^2\beta_n}}\right], \tag{3-7}$$

On the other hand, feed cutting force F_f can be found as,

$$F_f = R\sin(\beta_n - \alpha_n) \tag{3-8}$$

The resultant force R can be derived from Figure 3.3, plugging R into the equation 3-8 yields,

$$R = \frac{F_s}{\cos(\phi_n + \beta_n - \alpha_n)} \tag{3-9}$$

Plugging equation 3-9 into equation 3-8, F_f turns out to be,

$$F_f = \frac{F_s \sin(\beta_n - \alpha_n)}{\cos(\phi_n + \beta_n - \alpha_n}) \tag{3-10}$$

Lastly, substituting shear force F_s from equation 3-5 to equation 3-9, F_f can be derived as,

$$F_f = tb\left[\frac{\tau}{\sin\phi_n \cos i}\frac{\sin(\beta_n - \alpha_n)}{\sqrt{\cos^2(\phi_n + \beta_n - \alpha_n) + \tan^2\eta \sin^2\beta_n}}\right], \tag{3-11}$$

On the other hand, the radial force can be evaluated as,

$$\begin{aligned} F_r &= F_f \sin i - F_R \cos i \\ F_r &= F_S\left(\frac{\cos(\beta_n - \alpha_n)\cos F_S^{'} \sin i}{\cos(\phi_n + \beta_n - \alpha_n)} - \sin F_S^{'} \sin i\right. \end{aligned} \tag{3-12}$$

Substituting equation 3-4 and equation 3-5 in equation 3-12, radial force F_r is evaluated as,

$$F_r = tb\left[\frac{\tau}{\sin\phi_n}\frac{\cos(\beta_n-\alpha_n)\tan i-\tan\eta\sin\beta_n}{\sqrt{\cos^2(\phi_n+\beta_n-\alpha_n)+\tan^2\eta\sin^2\beta_n}}\right] \tag{3-13}$$

The most crucial part is the evaluation of the cutting variables shear stress (τ), normal shear angle (ϕ_n), normal friction angle (β_n) and chip flow angle (η). For shear angle there are two approaches, one of them is proposed by Merchant [1] and the other one is proposed by Armarego [8]. Merchant's theory is based on the minimum energy principle in orthogonal cutting and it can be extended to oblique cutting by geometrical relations. Armarego's approach is empirical approach in which contains two main assumptions.

i. The shear velocity is collinear with shear force
ii. The chip ratio in oblique cutting is the same as in the orthogonal cutting

In the light of these assumptions the normal shear angle (ϕ_n) can be obtained by:

$$\tan(\phi_n) = \frac{r_c(\cos\eta/\cos i)\cos\alpha_n}{1-r_c(\cos\eta/\cos i)\sin\alpha_n} \tag{3-14}$$

where r_c stands for the chip ratio, η is the chip flow angle and *i* is the oblique angle. If Stabler's chip flow angle rule ($\eta \equiv i$) is applied for a given tool geometry, the friction angle β_n can be derived from equation (3-14) and equation (3-21). However, considering the oblique cutting geometry, the friction angle can also be calculated from the oblique cutting tests in which F_t, F_f and F_r are identified. Since the three force components are known, friction force *F* and the normal force *N* can be obtained.

$$F = \sqrt{\left\{(F_t\cos i + F_r\sin i)\sin\alpha_n + F_f\cos\alpha_n\right\}^2 + (F_t\sin i - F_r\cos i)^2} \tag{3-15}$$

$$N = (F_t\cos i + F_r\sin i)\cos\alpha_n - F_f\sin\alpha_n \tag{3-16}$$

Therefore, the friction angle can be determined by coefficient of friction which is:

$$\mu = \frac{F}{N} = \tan\beta$$

$$\tan\beta = \frac{\sqrt{\left\{\left(F_t\cos i + F_r\sin i\right)\sin\alpha_n + F_f\cos\alpha_n\right\}^2 + \left(F_t\sin i - F_r\cos i\right)^2}}{\left[F_t\cos i + F_r\sin i\right]\cos\alpha_n - F_f\sin\alpha_n} \tag{3-17}$$

The shear force and shear area can also be identified from the oblique cutting tests. Hence, shear stress (τ) can be obtained by:

$$\tau = \frac{F_s}{A_s}$$

$$\tau = \frac{\sqrt{\left\{\left(F_t\cos i + F_r\sin i\right)\cos\phi_n - F_f\sin\phi_n\right\}^2 + \left(F_t\sin i - F_r\cos i\right)^2}\cos i\sin\phi_n}{tb} \tag{3-18}$$

The other important parameter in oblique cutting is the chip flow angle. In order to determine the chip flow angle numerical approaches were developed. Stabler [6] analyzed the oblique cutting geometry and proposed a widely accepted a chip flow law *Stabler's rule*. According to this law the chip flow angle is assumed to be equal to the angle of obliquity, which is a great assumption and does not take the effect of shear angle, friction and rake angle during cutting. Hence, depending on the cutting conditions Stabler's rule may cause major errors in the cutting force predictions especially for the extreme cases of tool geometry. On the other hand, Merchant [1] proposed the equation 3-19 for shear velocity considering the effect of oblique angle which will lead the chip flow angle with another formulation developed by Stabler [6] for the shear force (equation (3-20)). Assuming the shear force and shear velocity are being equal the equation (3-21) is developed by Armarego and Brown [8].

$$\tan\delta_v = \frac{\tan i\cos(\phi_n - \alpha) - \tan\eta\sin\phi_n}{\cos\alpha_n} \tag{3-19}$$

$$\tan\delta_f = \frac{\sin\beta\sin\eta}{\cos\beta\cos(\phi_n - \alpha_n) - \cos i\sin\beta\sin(\phi_n - \alpha_n)} \tag{3-20}$$

$$\tan(\phi_n + \beta_n) = \frac{\cos\alpha_n\tan i}{\tan\eta - \sin\alpha_n\tan i} \tag{3-21}$$

Solving equation (3-21) and equation (3-14) together will yield a formulation for chip flow angle. The resulting equation can be put into the following form:

$$A\sin\eta - B\cos\eta - C\sin\eta\cos\eta + D\cos^2\eta = E$$

where

$$\begin{aligned} \text{A} &= r\cos\alpha_n + \cos i\tan\beta \\ \text{B} &= \tan\beta\sin\alpha_n\sin i \\ \text{C} &= r\sin\alpha_n\tan\beta \\ \text{D} &= r\tan\beta\tan i \\ \text{E} &= \sin i\cos\alpha_n \end{aligned} \tag{3-22}$$

Equation (3-22) is numerically solved for chip flow angle (η_c). The solution method is a medium-scale algorithm and uses the trust-region dogleg method [31] which is implemented under *fsolve* function in Matlab[1]. This method is one way of solving the system of non-linear equations, depending on the solution procedure the solution accuracy changes.

Analytical solutions for the chip flow angle can be verified by experimental measurement of chip flow direction. A number of techniques can be used such as marking tool with dye, which will not give very accurate results, or taking pictures of chip while it flows through the rake face. The second method will capture instantaneous movement of chips and fluctuation on the rake face, which is why this method is more reliable than marking tool with dye technique.

[1] Matlab is a trademark of The MathWorks, Inc

The other approach for the prediction of oblique cutting forces is the transformation from the orthogonal cutting database in the light of following assumptions [7]. After the evaluation of the shear angle (ϕ), friction angle (β) and shear stress (τ) from orthogonal cutting tests, the orthogonal shear angle is assumed to be equal to the normal shear angle in oblique cutting ($\phi \equiv \phi_n$); the second assumption is normal rake angle in oblique cutting is equal to the rake angle in orthogonal cutting ($\alpha \equiv \alpha_n$) and third assumption is based on Stabler's chip flow angle rule [6] which is equal to the angle of obliquity ($\eta \equiv i$). Besides this parameters the friction angle (β) and shear stress (τ) can be taken as the same in both orthogonal cutting and oblique cutting. Then the force prediction can be done by plugging the transformed parameters into equations 3-7, 3-11 and 3-13.

3.2 Experimental Analysis on Oblique Cutting

The mechanics and the fundamental parameters of the oblique cutting are presented in Chapter 3. In this section, the experimental verification of oblique cutting parameters for Ti_6Al_4V alloy is demonstrated for different cutting conditions. Also, transformation of cutting force coefficients from the orthogonal model to oblique model is compared with the experimental results.

Oblique cutting tests are conducted on Ti_6Al_4V alloy for different tool geometries and cutting parameters. Ti_6Al_4V oblique cutting tests are conducted at dry conditions with 3-10 m/min speed range and 0.06 – 0.18 mm/rev feed rate range for 7° and 11° inclination angles. Normal shear angle, shear stress, friction angle and cutting force coefficients are obtained from experiments. Obtained results are compared with the orthogonal cutting tests. In addition, cutting force coefficients are transformed from orthogonal cutting tests and compared with the oblique cutting results. A good agreement between measured and transformed data is observed. Also, the different methods regarding the chip flow angle determination is applied and obtained results are compared. The first method is the application of Stabler's rule, which assumes the chip flow angle is equal to the oblique angle. In the second method, analytical formulation (see Equation 3-22) is used and finally

third method was direct measurement of chip flow angle from the experiments by using video recordings.

The data given below are the comparisons of the normal shear angle, the shear stress, the friction angle and the cutting force coefficients measured from Ti_6Al_4V orthogonal and oblique cutting tests.

Normal Shear Angle in Ti_6Al_4V Oblique Cutting Tests:

Shear angle determines the orientation of shear plane in orthogonal and oblique cutting. However, in oblique cutting existence of the inclination angle affects the shear plane orientation. As it is explained in Chapter 2.2, shear angle in the normal plane is considered in experimental analysis. The following Figure 2.33.a shows the variation in normal shear angle with feed rate in orthogonal and oblique cutting tests.

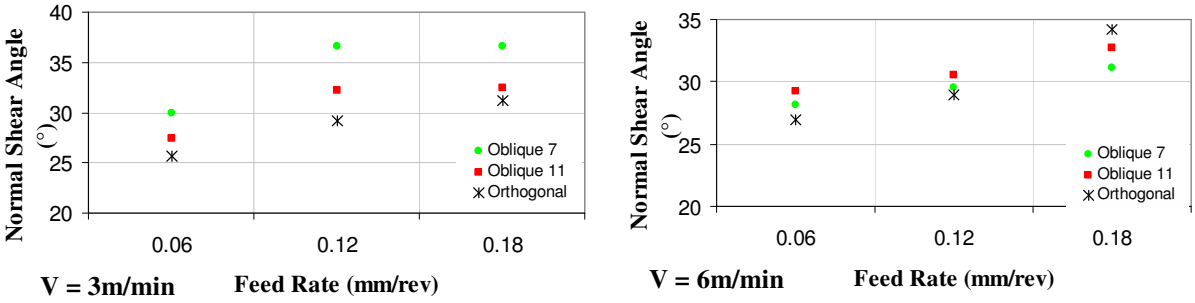

Figure 3.5: Variation of normal shear angle with feed rate for different cutting speeds in orthogonal and oblique cutting.

Figure 3.5.a and Figure 3.5.b show the variation in normal shear angle with feed rate in orthogonal and oblique cutting tests. In both tests shear angle shows the same trend and increased as the feed rate increases. This is an expected result due to the increase in the chip ratio as the feed rate increases. Also, increase in the cutting speed does not affect the normal shear angle significantly for oblique cutting. Therefore, it can be deduced that shear angle is a function of feed rate for orthogonal and oblique cutting.

Normal Friction Angle in Ti_6Al_4V Oblique Cutting Tests:

In oblique cutting, due to the inclination angle, chip formation occurs in three dimensions. Therefore, interaction between the cutting tool and chip changes and affects the friction coefficient during cutting. This fact is investigated in oblique cutting experiments and results are presented in Figure 3.6. It is observed that the friction angle changes with the feed rate, and there is a slight difference between the orthogonal and oblique friction angles due to the obliquity. However, the general trend in friction angle for oblique and orthogonal cutting is nearly the same. Therefore, it can be concluded that cutting speed and feed rate does not have any significant effect on friction angle. As it is presented in Chapter 2, the friction angle is only affected by rake angle.

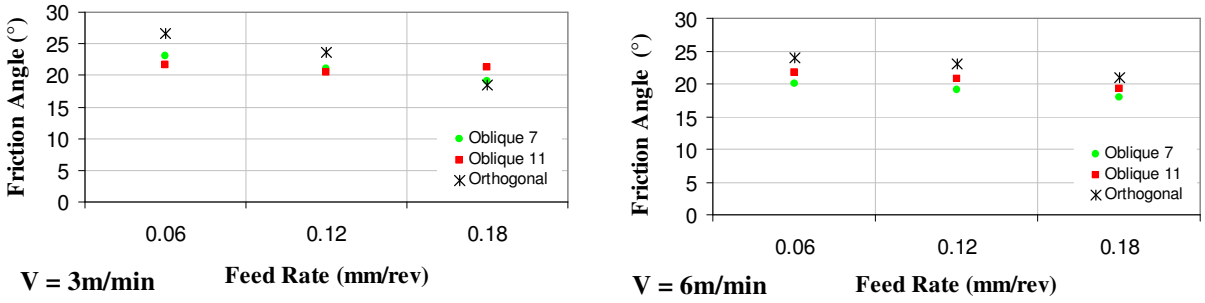

Figure 3.6: Variation of friction angle with feed rate for different cutting speeds in orthogonal and oblique cutting.

Shear Stress in Ti_6Al_4V Oblique Cutting Tests:

Figure 3.7 shows the effect of feed rate on shear stress; however as the feed rate increases shear stress does not vary significantly. Therefore, it can be said that shear stress is not depended on feed rate. The orthogonal cutting tests conducted before showed that only the rake angle affects the shear stress significantly.

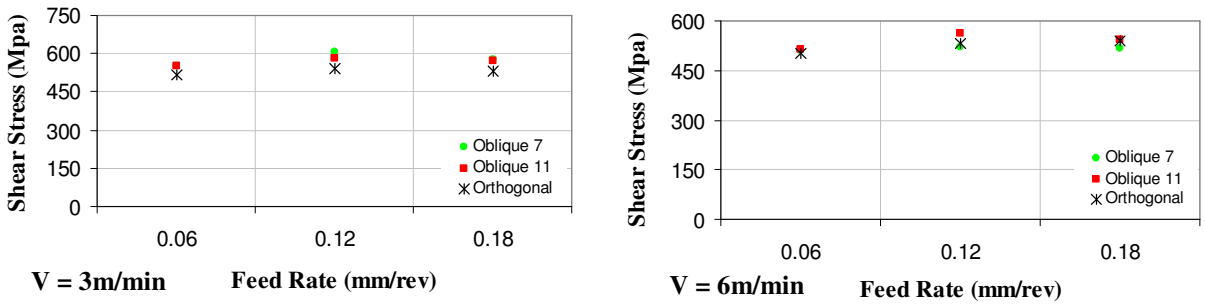

(a) (b)

Figure 3.7 : Variation of shear stress with feed rate for different cutting speeds in orthogonal and oblique cutting.

Cutting Force Coefficients in Ti_6Al_4V Oblique Cutting Tests:

Cutting force coefficients are used in force calculations in cutting process in the following form:

$$F_t = K_{tc} bt$$
$$F_f = K_{fc} bt \qquad (3\text{-}23)$$
$$F_r = K_{rc} bt$$

For a given depth of cut b, and uncut chip thickness t, force coefficients can be determined from the experiments by dividing measured forces to the chip area. However, it should be noted that measured forces contain edge forces and should be excluded in the cutting force coefficient calculation. The following graphs represent the behavior of cutting force coefficients in Ti_6Al_4V oblique cutting tests. Obtained oblique cutting coefficients are compared with orthogonal cutting coefficients.

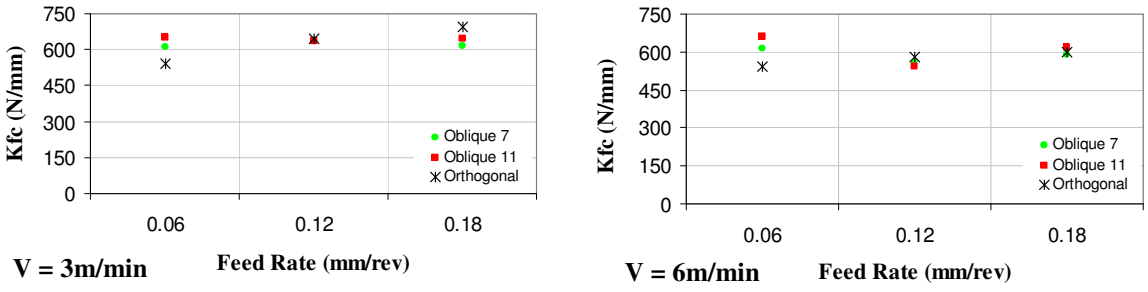

(a) (b)

Figure 3.8: Variation of feed cutting force coefficient with feed rate for different cutting speeds in orthogonal and oblique cutting for Ti_6Al_4V

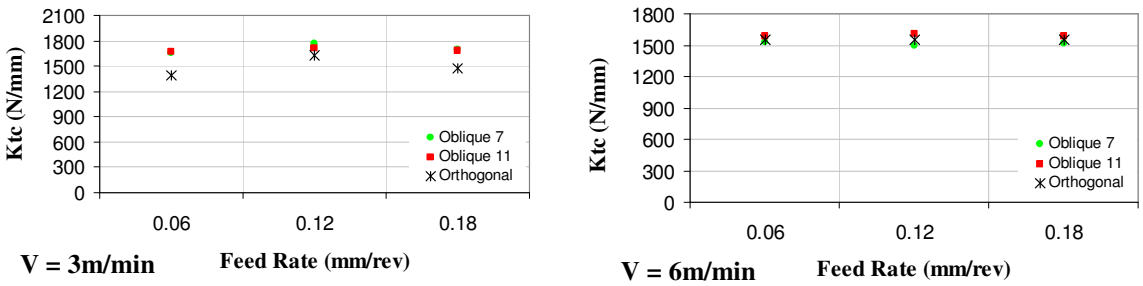

Figure 3.9: Variation of tangential cutting force coefficient with feed rate for different cutting speeds in orthogonal and oblique cutting for Ti_6Al_4V.

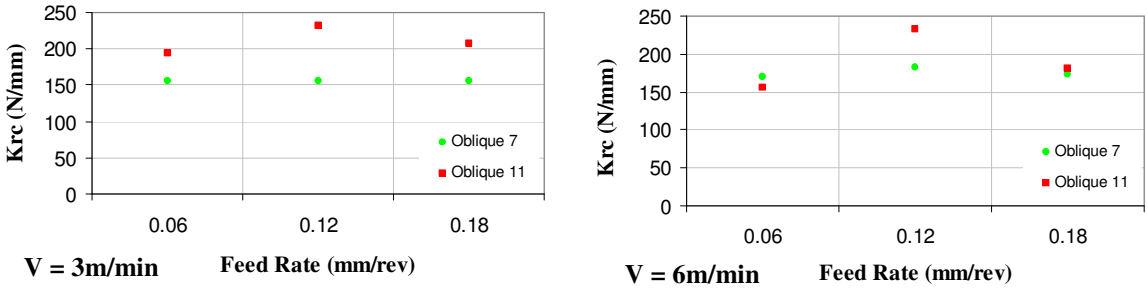

Figure 3.10: Variation of radial cutting force coefficient with feed rate for different cutting speeds in orthogonal and oblique cutting for Ti_6Al_4V.

Figures 3.10, 3.11 and 3.12 show the effect of feed rate and cutting speed to the cutting force coefficients. As it can be observed effect of increasing feed rate yield different results in cutting force coefficients. This is the consequence of edge forces during cutting. Since the cutting tool is sharp, variation in the edge forces increase, therefore cutting force coefficients fluctuate.

Oblique Cutting Transformation and Chip Flow Angle Prediction:

As it is presented in the beginning of this chapter, oblique cutting force coefficients can also be evaluated by transformation from the orthogonal data. In the transformation procedure there are main assumptions such as rake angle, shear angle, friction angle and shear stress are assumed to be equal to the normal rake angle, normal shear angle, friction coefficient and shear stress in oblique cutting respectively. In addition to that, as Stabler proposed [6] the chip flow angle η_c is assumed to be equal to the inclination angle *i*, in the

oblique transformation of cutting coefficients. However, beside the Stabler's chip flow rule, the chip flow angle is determined by two additional methods and results are presented. In the first method, chip flow angle is determined by capturing snapshots from video recordings taken during cutting and the second method is to predict it analytically (see Equation 3-22). Figure 3.11 shows a snapshot taken from oblique cutting and Figure 3.12 shows the comparison between predicted chip flow angle and measured chip flow angle.

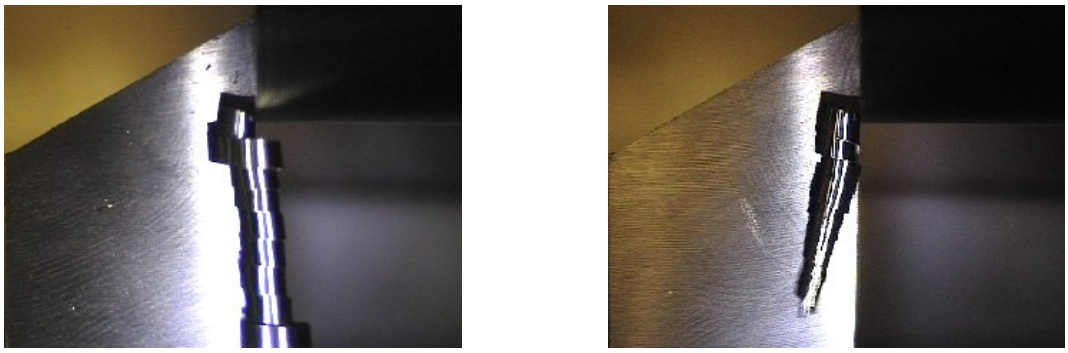

(a) (b)

Figure 3.11: A snapshot from oblique cutting, inclination angle 11°

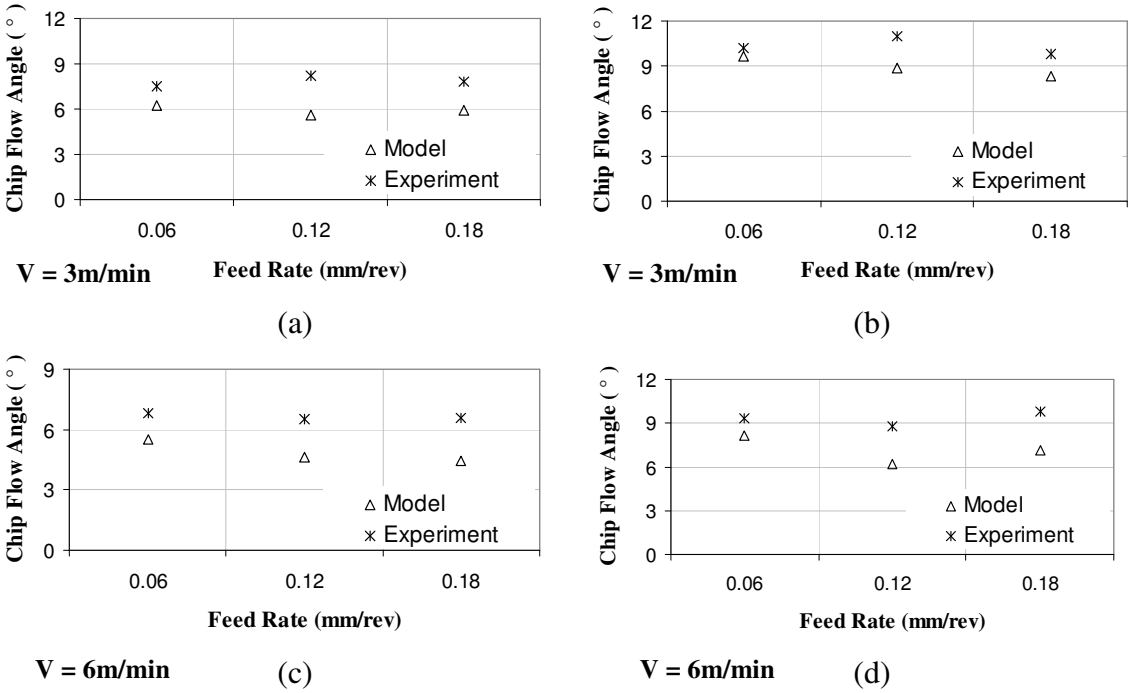

Figure 3.12: Comparison of chip flow angle by the proposed model and experiments for Ti_6Al_4V alloy with HSS cutting tools having inclination angles of (a)-(c) 7°, and (b)-(d) 11°.

The average error between experimental results and model predictions is found to be 18% and 10% for inclination angles of 7° and 11° respectively. Another observation from chip flow angle measurements in Ti_6Al_4V oblique cutting is that as the cutting speed increases measured chip flow angle also increases. This is due to a reduction in coefficient of friction as the cutting speed increases. More precisely, increase in the cutting speed increases the temperature so as the contact length on the rake face; therefore mean coefficient of friction is decreasing as the cutting speed increases.

On the other hand, oblique transformation method is verified by Ti_6Al_4V oblique and orthogonal cutting tests. Shear angle, friction angle and shear stress values are taken from the orthogonal cutting tests and transformation procedure is applied. Then, the results obtained from oblique transformation are compared to the cutting force coefficients in oblique cutting tests. Average errors are found 10 %, 10% and 23% for K_{fc}, K_{tc} and K_{rc} respectively. The following figures show the comparison between the measured and transformed cutting force coefficients with measured chip flow angle.

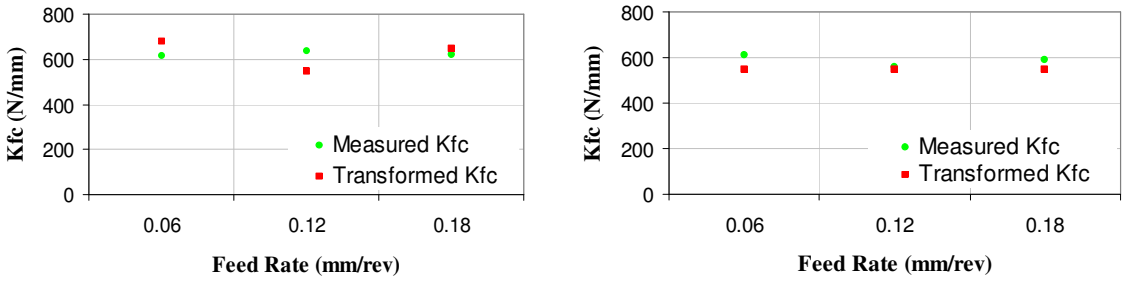

Figure 3.13: Comparison of measured feed cutting force coefficient and transformed feed cutting force coefficient with feed rate in Ti_6Al_4V oblique cutting.

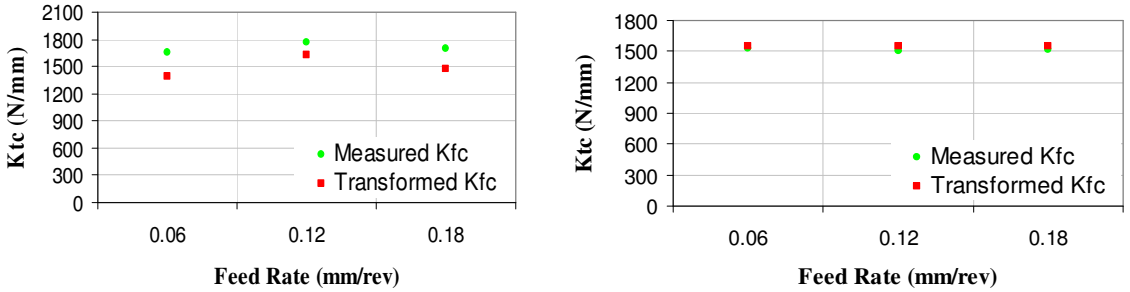

Figure 3.14: Comparison of measured tangential cutting force coefficient and transformed tangential cutting force coefficient with feed rate in Ti_6Al_4V oblique cutting.

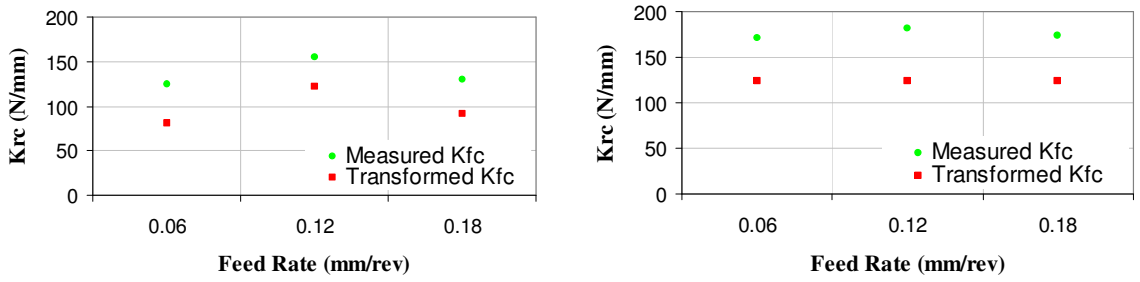

Figure 3.15: Comparison of measured radial cutting force coefficient and transformed radial cutting force coefficient with feed rate in Ti_6Al_4V oblique cutting.

Also, the error rates between Ti_6Al_4V oblique cutting force coefficients by using different chip flow angle measurement methods are presented.

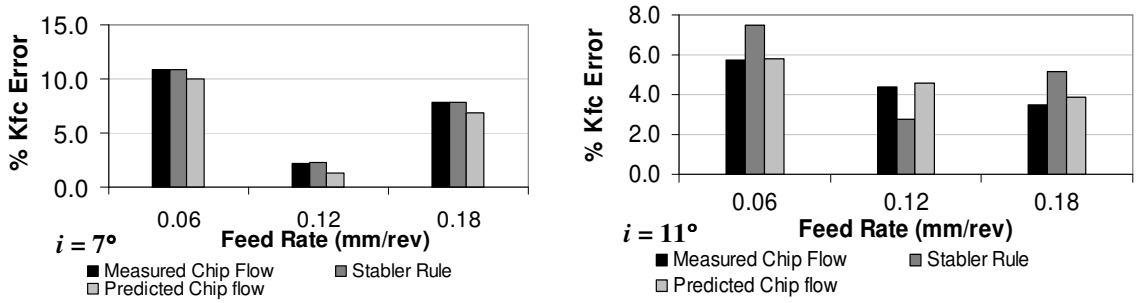

Figure 3.16 : Percentage errors in oblique cutting feed force coefficients for different chip measurement methods.

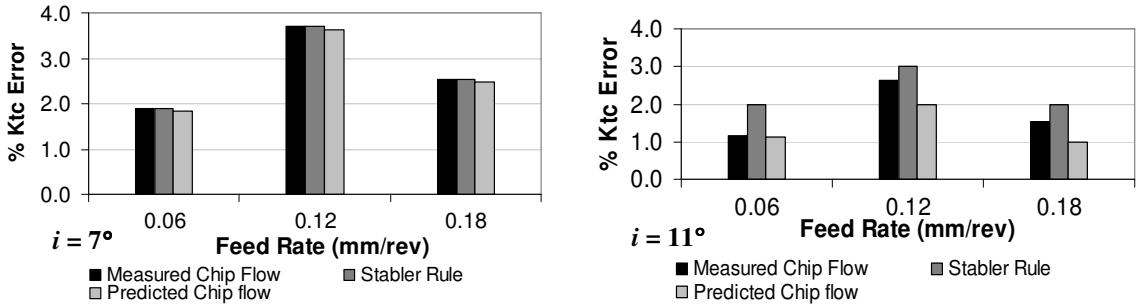

Figure 3.17 : Percentage errors in oblique cutting tangential force coefficients for different chip measurement methods.

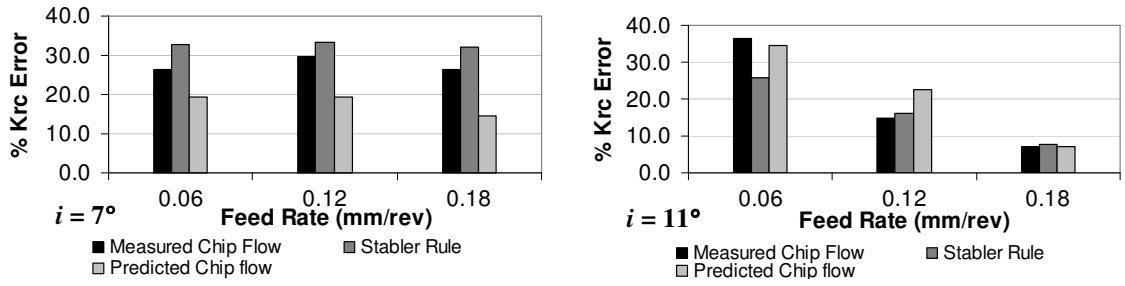

Figure 3.18: Percentage errors in oblique cutting radial force coefficients for different chip measurement methods.

According to the results obtained from oblique cutting tests with different chip flow angle measurements, it can be deduced that for larger inclination angle analytical chip flow angle calculation performed better than the other chip flow angle measurement methods. Since, Stabler's chip flow rule does not consider the effect of shear angle, friction and tool geometry, larger error rates are introduced for most of the cases. Depending on the cutting conditions and the quality of the video recording, the performance of the measured chip flow angle changes. In our case, this method performed well, however analytical chip flow angle prediction introduced the lowest percentage errors.

To sum up, in this chapter the oblique cutting experiments with different chip flow determination methods for Ti_6Al_4V titanium alloy under different cutting conditions are conducted. Also, oblique cutting force coefficients are transformed from the orthogonal data and as expected good agreement is observed between transformed force coefficients and measured force coefficients. This results implies that, under certain assumptions modeling of the complex cutting operations can possible by conducting orthogonal cutting tests.

CHAPTER 4

ANALYSIS AND MODELING OF EDGE FORCES IN ORTHOGONAL CUTTING

The cutting tool edge geometry is one of the most important parameters in machining operations. If the cutting edge is sharp or the hone radius is small compared to the feed rate, the cutting forces will be mainly due to the primary and the secondary deformation zones, and thus the effect of the hone on the cutting forces will be minimal. However, cutting tools in practice have noticeable hone radii which are generally comparable to feed rates. That's why the hone radius becomes critical for accurate prediction of the cutting forces due to the third deformation zone which is responsible for the edge cutting forces. The edge cutting forces can be relatively high when the uncut chip thickness is comparable with the hone radius. Tool with larger hone radii are more resistant to chipping, and dampen the vibrations while cutting [10] which indicates that the hone radius is inevitable.

4.1 Modeling Approach

In this section, an initial process model that takes the hone radius into account is presented [20]. Although the details of the model can be found in [20] in detail, a very brief review will be given here. The proposed approach in this study is an initial model that covers the primary and secondary shear zones in an accurate manner, which also models the behavior at the third deformation zones. However, the model is still under development for the flank contact length predictions.

The hone radius (see Figure 4.1) on cutting tools affects the deformation in two ways. Firstly, the contact at the rake face is no longer a straight path aligned with the rake face,

but a curved path. Secondly, the hone results in another deformation zone which is due to the ploughing and the clearance contact.

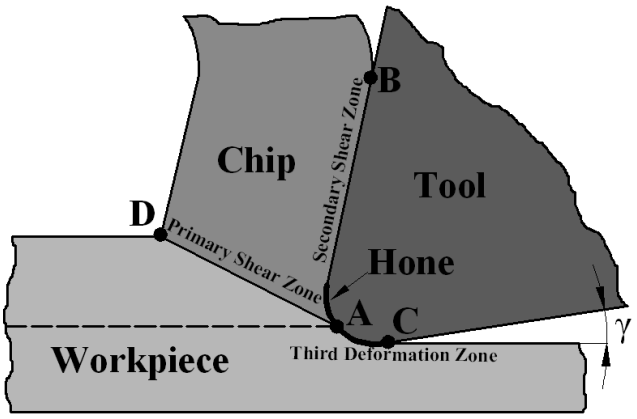

Figure 4.1: The hone and the deformation zones in orthogonal cutting.

In Figure 4.1, the deformation zones in orthogonal cutting are presented. The primary shear zone (AD), and the secondary shear zone (AB) are responsible for the chip formation where, hone radius below point A (AC) is responsible for the ploughing and the clearance contact. In the model it is assumed that the point A is a stagnation point where the material just above it moves upwards contributing to the chip formation. The material just below point A moves downwards and continues contact with the path AC.

Although the model proposed here can be used with any primary shear zone model, the approach used by Molinari et al. [21] is selected, and the contact zones are divided into several regions as can be seen in Figure 4.1. The division is made so that the minimum number of regions is obtained to achieve simplification in the derivation and faster solution times.

The region (AB), shown in Figure 4.2 which is responsible for the contact between the chip and the tool is divided into three regions. It should be noted here that, due to the hone radius, the rake contact is not a straight line anymore but a straight line plus a curved path. Because of this, the direction of the normal and friction forces on the rake contact is varying along each region except region 1 which is a straight path. Thus, a straight rake contact is defined in region 1. Although region 2 and 3 in Figure 4.2 can be merged, for the simplification in the mathematical representation they are taken as two different regions.

The path (AC), on the other hand, is divided into two regions, as shown in Figure 4.2. Region 4 is the region responsible for the material having plastic deformation before entering region 5 where flank contact occurs.

Basically, the proposed approach does not model the material deformation in front of the hone radius directly, but it assumes pressure and shear stress distributions at the contact between the tool and the workpiece on path AC. On the other hand, the true analysis of Region 5 needs the knowledge of deformation zone in front of the hone radius.

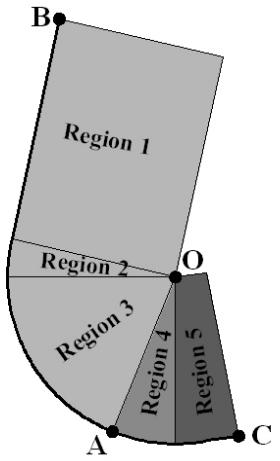

Figure 4.2: The regions used in edge force modeling.

4.1.1 Modeling of the Primary Shear Zone

Although the model proposed here can be used with any primary shear zone model, the approach used by Molinari et al. [21] is adapted. The main assumption is that the primary shear zone has a constant thickness, and that no plastic deformation occurs before and after the primary shear zone up to the sticking region on the rake face. The material behavior is represented with the Johnson-Cook constitutive model in this study.

The material entering the primary shear zone sustains a shear stress of τ_0. The shear stress at the exit of the shear plane, τ_1 is different from τ_0 when inertia effects are important. Assuming a uniform pressure distribution along the shear plane (exit of the primary shear zone), τ_0 can be iteratively calculated as proposed in [22]. From the conversation of momentum we obtain [22]:

$$\tau_1 = \rho(V \sin\phi)^2 \gamma_1 + \tau_0 \tag{4-1}$$

where ρ is the density of the workpiece material γ_1 is the plastic shear strain at the exit of the primary shear zone, V is the cutting speed and ϕ is the shear angle.

4.1.2 Modeling of the Secondary and Third Deformation Zone

Once the material leaves the primary shear band it is exerted with a very high normal pressure at the cutting tool tip which results in sticking (plastic) friction conditions at those regions close to the tool tip. Due to the drop in the normal pressure the friction conditions turn to sliding (elastic). This contact phenomenon is first observed by Zorev [23]. As for the third deformation zone, when the material, which doesn't contribute to the chip formation has the initial contact with the hone i.e. Region 4, again due to the very high normal pressure the friction conditions are assumed to be sticking. It is assumed in this study that once the material leaves region 4 and makes a contact with region 5 due to the elastic recovery, the friction state turns to completely sliding.

Therefore, due to the complicated contact conditions, in modeling of the secondary and third deformation zones, the friction behavior of the material is critical. In a previous study [24] it was proposed to calibrate the sliding friction coefficient between the tool and the workpiece materials by few numbers of orthogonal cutting tests. In order to model the contact behavior, on the other hand, the normal and shear stress distributions are assumed as in Figure 4.3. The pressure and shear stress distributions in regions 1, 2 and 3 were observed before by split-tool cutting tests [26, 27].

Using the proposed distributions and the force equilibrium on the chip, the formulations for the length of the sticking and sliding contacts can be derived. By applying the moment equilibrium at the tool tip the total contact length on the rake face can be

calculated. Also from the stress distribution, the sticking contact length can be calculated as follows [24]:

$$\ell_p = \ell_c \left(-\left(\frac{\tau_1}{P_0 \mu} \right)^{1/\zeta} + 1 \right) \tag{4-2}$$

where ℓ_p is the sticking contact length, ℓ_c is the total contact length at the rake, P_0 is the normal pressure at the stagnation point, μ is the sliding friction coefficient, and ζ is the distribution exponent.

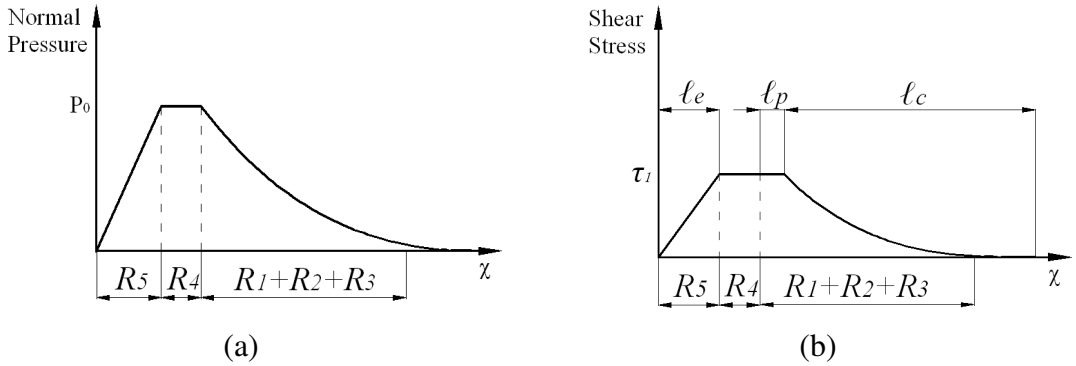

Figure 4.3: (a) The normal pressure and (b) the shear stress distributions on the contact regions.

The region 5 is responsible for the workpiece material which doesn't contribute to the chip flow. It is also experimentally observed that the contact with the workpiece material continues along this region which is called the flank contact. The flank contact is due to the elastic recovery of the material deformed in front of region 4. The proposed model in this study doesn't consider the deformation areas in the material, but assumes pressure and shear stress distributions at the contact. Therefore, without any further information, the proposed model cannot predict the contact length at the clearance face, and thus the cutting forces properly. In order to overcome this difficulty we use contact length measurements on the flank face which are compared with the cutting force results.

4.1.3 Stagnation Point, Shear Angle and Cutting Forces

The stagnation point position is one of the key parameters in defining the contact regions. The stagnation is assumed to occur at point *A* where the line connecting it to the center of the hone has θ_s degrees with the vertical axis (see Figure 4.4). In the previous studies [15,16] it has been shown that θ_s for metals is approximately in the range of 25º-30º. However, for the cases where shear angle is bigger than θ_s, there is geometrical conflict between the hone radius and the shear band. For instance, shear plane *AD* will always have a conflict with the hone if the shear angle is greater than θ_s. In order to avoid this conflict, the minimum value of the θ_s must be equal to the shear angle. For this reason, θ_s is assumed to be equal to the shear angle in this study i.e. $\phi = \theta_s$. This is justified by the shear angle measurements for steels which are in the range of 25º-35º in typical cutting processes [20].

The shear angle ϕ is calculated by minimization of the cutting energy. It is determined by running a simulation program based on the proposed model for a given range of shear angles, and the one that corresponds to the minimum cutting power is selected as the shear angle [20, 28]. Although the primary, secondary and third deformation zones are modeled separately, they are coupled through the shear angle.

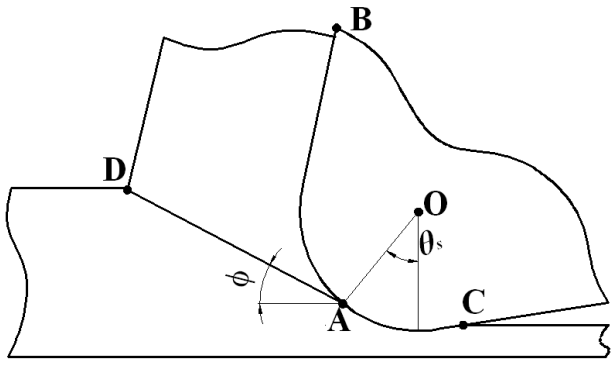

Figure 4.4: The stagnation point, and the shear angle ϕ.

The cutting forces can be obtained by the force equilibrium on the chip as follows [20]:

$$F_c = \tau_1 \frac{wh_1}{\sin\phi} \frac{\cos(\lambda_a - c)}{\cos(\phi + \lambda_a - c)}$$
$$F_f = \tau_1 \frac{wh_1}{\sin\phi} \frac{\sin(\lambda_a - c)}{\cos(\phi + \lambda_a - c)} \quad (4\text{-}3)$$

where F_f is the feed and F_c is the tangential cutting forces. Note that the cutting forces in equation (4-3) don't include the forces acting on region 4. Therefore, these forces should also be added in order to obtain the total cutting forces.

4.2 Experimental Verification and Investigation

In this section, experimental results that are used for verification are presented. The results are also compared with the FEM predictions. Also the experimental results are discussed in explaining the cutting mechanics at the hone region.

4.2.1 Test Procedure

A series of orthogonal cutting experiments were conducted on a turning center with AISI 1050 steel tubular workpiece. The machining forces were measured by a table type dynamometer mounted on the turret. The edge radius and clearance angle affect the cutting process and edge forces. Hence, in order to see the edge force effect a detailed experimental investigation consisting of four factors was conducted. Table 4-1 summarizes the cutting parameters of investigations.

Cutting Speed (m/min)	250
Feed Rate (mm/rev)	0.05, 0.1, 0.15, 0.2
Clearance Angle (º)	3 , 7, 11
Edge Radius (mm)	0.012, 0.03, 0.06

Table 4-1 Cutting Parameters

All tests are conducted at dry conditions at 2 mm depth of cut. In each test, cut chip thicknesses were measured using two different methods. In the first measurement technique, the chip thickness is measured by a micrometer, where in the second method weight measurement is used for determining the chip thickness. In order to determine the edge forces, the measured tangential and feed forces are plotted against the feed rate, and the force intercept using linear regression is determined as tangential and feed edge force components, respectively.

Another important parameter for the proposed model is the flank contact length. After each cutting test the flank contact is measured by microscope. In the measurements it is important to look perpendicular to the flank face; therefore a fixture which makes the clearance angle zero is built. Figure 4.5 shows a sample measurement image regarding the flank contact length.

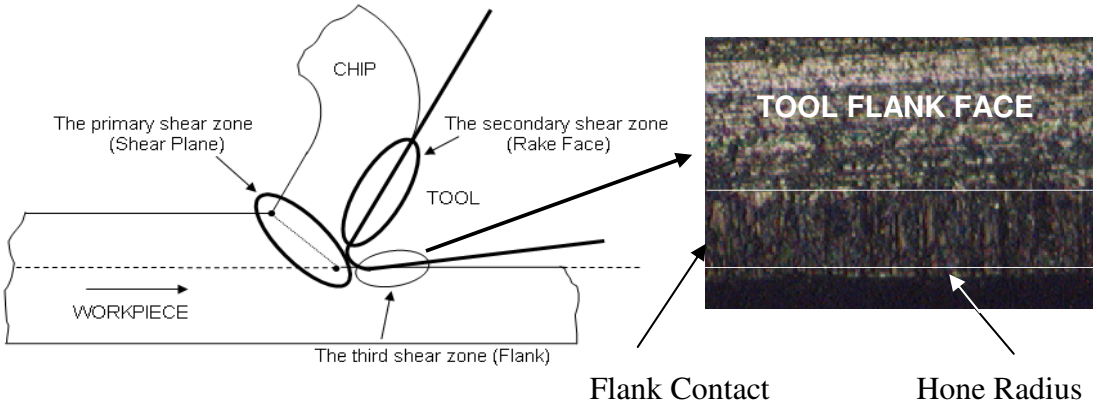

Figure 4.5: Orthogonal cutting geometry and flank contact visualization (top view of flank).

4.2.2 Comparison of the Analytical, FEA and Experimental Results

In this section the predictions of the proposed model are compared with the experimental and FEA results. The contact length on the flank face is obtained by the experimental measurements on the insert after the each cutting test as presented at the previous section. The measured flank contact values are used as an input in prediction of

the cutting forces. In addition, a FEA is conducted based on test conditions using a commercial software package, and the force results are compared with analytical and experimental results. The FEA is based on an updated Lagrangian formulation for large plastic deformation analysis. The chip generation process was simulated as elasto-plastic conditions with continuous re-meshing. The friction factor during the simulations was taken as 0.7 after several trials. The simulation results yield cutting forces, stress distribution and contact length on the flank face. An example case can be seen in Figure 4.6. The model predictions along with the FEA (for one case), and experimental results can be seen in Figures 4.7 and 4.8.

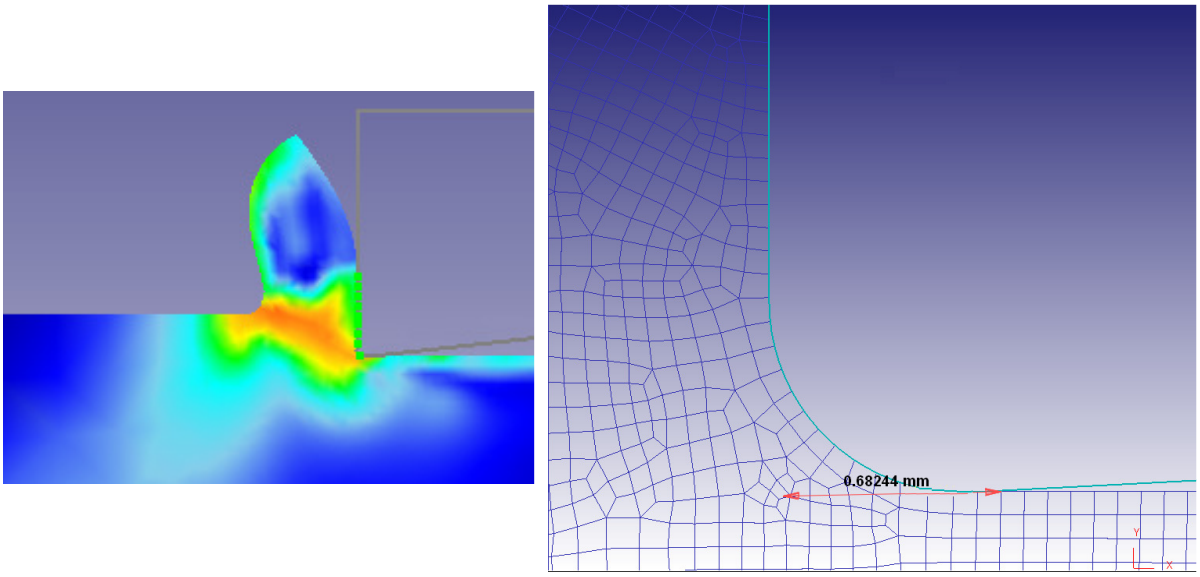

(a) (b)

Figure 4.6: (a) Stress and (b) flank contact length results from FEM software for feed rate of 0.15 mm/rev, cutting speed of 250 m/min, clearance angle of 3° and the hone radius of 60 µm.

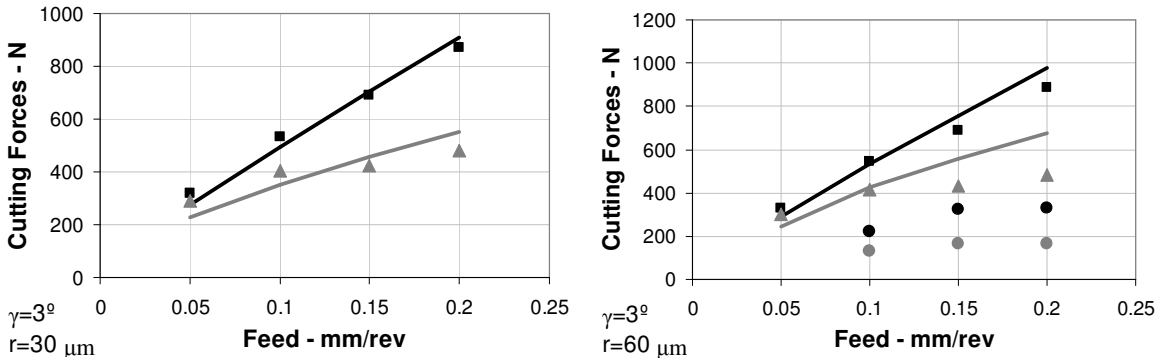

(a) (b)

Figure 4.7: Comparison of the feed (grey) and tangential (black) cutting forces obtained by the proposed model (lines), by FEM (circles) and measured from the experiments (markers) for insert having 3º clearance angle and hone radii of (a) 30 μm, and (b) 60 μm

The average discrepancy between the analytical model and the experimental results are 7% and 17% for the cutting and feed forces, respectively. The high discrepancy in the feed force predictions are related to the complicated contact on the flank face. The current model is still under development and the complicated behavior at the flank can be represented by the proposed model with further developments. However the verification results are promising for the proposed approach. The discrepancy between the FEA predictions and the experimental results, on the other hand, are very high while the predicted trend is in agreement with the experimental ones. This situation has also been observed in some previous studies [30]. The reason can be attributed to the inaccurate modeling of friction behavior in FEA analysis.

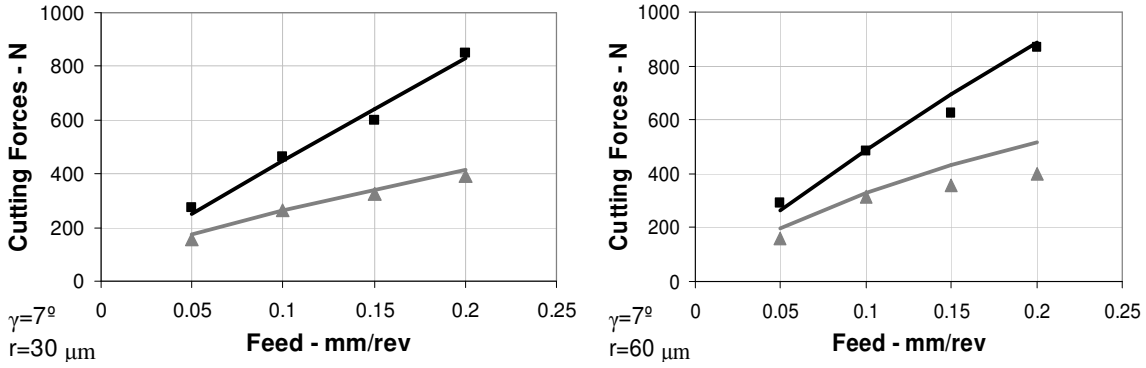

(a) (b)

Figure 4.8: Comparison of the feed (grey) and tangential (black) cutting forces obtained by the proposed model (lines) and measured from the experiments (markers) for insert having 7º clearance angle and hone radii of (a) 30 μm, and (b) 60 μm.

4.2.3 Experimental Investigations

Experimental comparisons are conducted in order to further discuss the effects of other process parameters such as edge hone radius and clearance angle on measured forces. Due to the deformation in the third shear zone, measured machining forces are affected by ploughing mechanism and include edge force component in both directions. The graphs given in Figure 4.9 are the observations from the AISI 1050 orthogonal cutting experiments, and show measured total cutting forces with respect to the edge radius. Figure 10, on the other hand shows the edge cutting forces with the varying hone radius. Once again it should be mentioned that the edge cutting forces are obtained by taking extrapolating the total cutting forces to 0 feed.

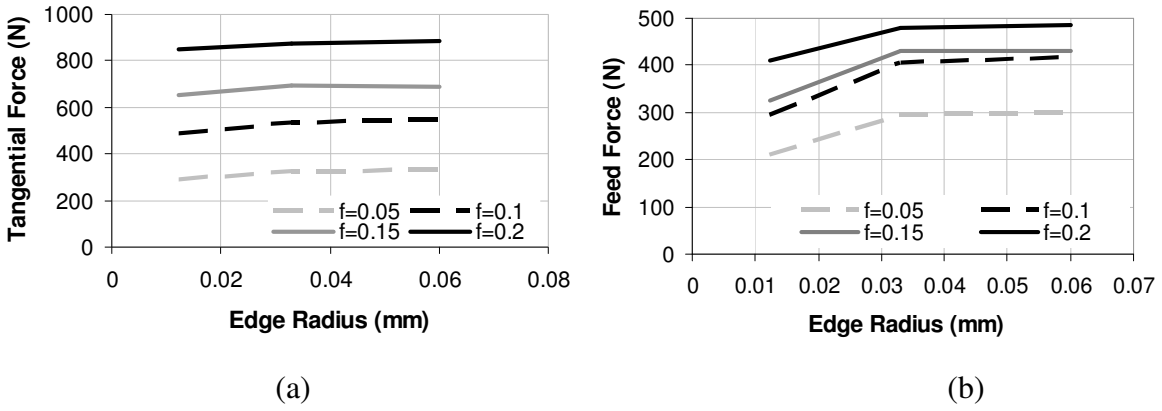

(a) (b)

Figure 4.9: Edge radius effect on (a) tangential and (b) feed cutting forces for cutting speed of 250 m/min and clearance angle of 3°.

Observing Figure 4.9 it can be deduced that the increase in the hone radius increases machining forces which is experimentally observed before [18, 29]. It is clear that the ploughing at the third deformation zone increases with the increasing hone radius which is the reason for increasing cutting forces. Another observation from Figure 4.9 is the non-linear trend of the cutting forces. As can be deduced from the results (Figures 4.9 and 4.10), increase in hone radius doesn't affect the cutting forces that much. For instance for the tests conducted with the tool having 11° clearance angle, although the hone radius is increased

from 30 μm to 60 μm (%100 increase), the feed forces increase from 180 N to 200 N (%11 increase) and tangential forces from 275 N to 290 N (% 5 increase). As it is discussed above, the increase in hone radius results in higher forces in cutting due to the higher ploughing. However, it is analytically and experimentally shown here that the fraction of increase in the hone radius doesn't directly reflect to the increase in the cutting forces. This behavior is also observed in the previous studies [18].

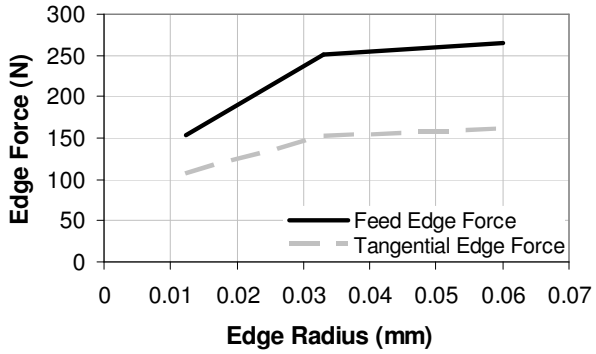

Figure 4.10: Edge radius effect on edge cutting forces for the clearance angle of 3º and , cutting speed of 250 m/min.

In addition, the edge force component of the total force for high hone radii is observed to be smaller than the ones for small hone radii as seen in Figure 4.10. However, there is a non-linear effect. For instance, when the hone radius increases from 12 μm to 30 μm the feed edge force increases 40% where there is 8% increase when the hone radius increase from 30 μm to 60 μm. On the other hand, it is apparent that for high feed rates the edge force component among the total cutting force is always smaller. For example, the tangential force in the case with the 3º of clearance and 60 μm hone radius is about 875 N and the corresponding edge force component is about 250 N. Hence, edge force constitutes 35% of the total tangential force. For the smallest feed rate, the measured tangential force is about 350 N and the feed edge force component is 250 N which is 60% of total tangential force. Therefore, modeling of the edge cutting forces is particularly critical for processes at small feed rates, i.e. finish and precision cutting operations, and for the cutting tools with large hone radii.

The clearance angle on the cutting tool is an important factor which has a direct effect on the flank contact length. Figure 4.11 below shows the relation between the clearance angle and measured forces during orthogonal cutting tests.

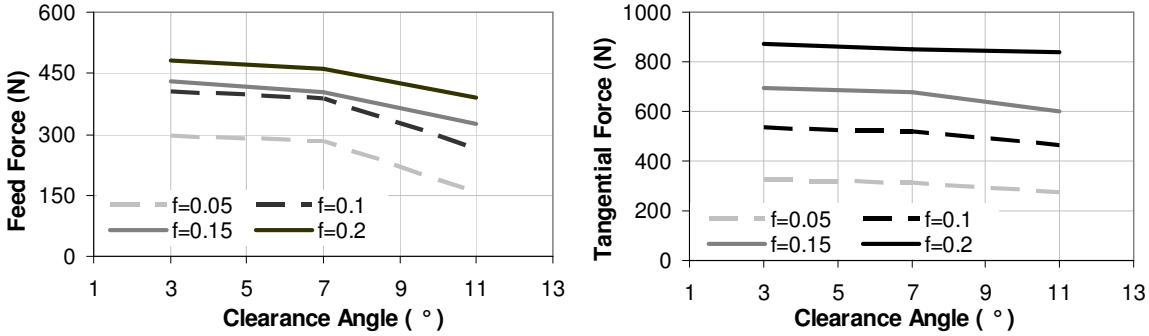

(a) (b)

Figure 4.11: Clearance angle effect on the feed and the tangential forces for the cutting speed of 250 m/min and hone radius of 30 µm.

The flank contact, on the other hand, needs to be observed in order to understand the true mechanical behavior at the third deformation zone. The measured flank contact values are given with respect to different values of clearance angle in Figure 4.12.

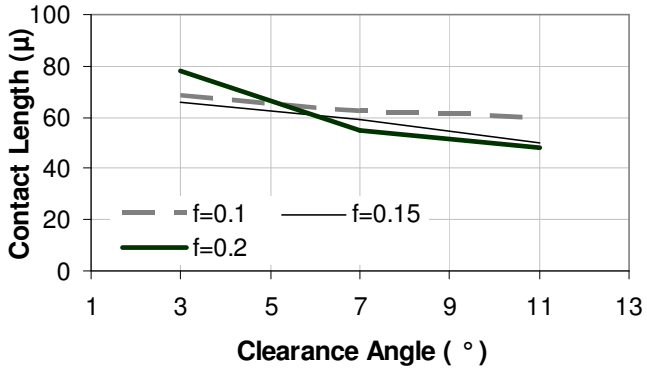

Figure 4.12: Clearance angle effect on flank contact length for the cutting speed of 250 m/min and hone radius of 60 µm.

It is analytically and experimentally (Figures 4.9 and 4.11) observed that increase in the clearance angle results lower measured forces in both feed and tangential cutting directions. Similar to the hone radius effect, the clearance angle variation doesn't affect the cutting forces in the same level. The reason of the decreased forces with respect to clearance angle is explained by the tool contact length in the flank face. The flank contact

decreases with the increasing clearance angle as can be seen in Figure 4.12. It is due to the elasto-plastic deformation mechanism at the flank face during cutting. For smaller values of clearance angle, tool flank becomes very close to the workpiece and elastic recovery of the workpiece creates larger flank contacts. On the other hand in higher clearance angle values tool flank is more separated from the machined surface, therefore elastic recovery of the workpiece generates smaller flank contacts.

CHAPTER 5 DISCUSSION AND CONCLUSION

In this thesis, the mechanics of metal cutting is reviewed and experimental investigation on orthogonal and oblique cutting is demonstrated for different materials and cutting conditions. Also, effect of the hone radius on the cutting process is investigated and cutting forces are predicted with the initial analytical force prediction model proposed by Ozlu [20].

In Chapter 2 and Chapter 3, mechanics of metal cutting is reviewed and experimental analysis of orthogonal and oblique cutting is conducted. The effect of process parameters for oblique and orthogonal cutting is discussed thoroughly for different materials, such as AISI 4340 and Ti_6Al_4V. Also, by using mechanistic approach the cutting forces are predicted and promising results are obtained under different cutting conditions. The following are the specific observations from experimental analysis:

- The cutting forces increase with the increasing feed rate and decreases with increasing cutting speed for both orthogonal and oblique cutting. Similarly, shear angle has an increasing trend with increasing feed rate and cutting speed due to the chip ratio and strain effect. On the other hand, friction angle has different outcomes for different materials. In AISI 4340 orthogonal tests, friction angle has a decreasing trend with cutting speed, where in Ti_6Al_4V orthogonal tests yield almost constant friction angle. This consequence is attributed to the physical properties of workpiece materials. Finally, shear stress is taking almost constant values with increasing cutting speed and feed rate. Only the rake angle changes the shear stress.

- Mechanistic modeling of cutting forces and orthogonal database for Ti_6Al_4V alloy is created. Cutting forces are predicted with mechanistic model and good agreement between the experiments and mechanistic model is found to be good. Average percentage errors are 13% and 10% for feed force and tangential force, respectively.

- Oblique cutting model is demonstrated for Ti_6Al_4V alloy with different cutting parameters and different chip flow angle measurement methods. Normal shear stress, friction angle and shear stress values are compared with different inclination angles and orthogonal data. It is observed that shear angle, friction angle and shear stress in oblique cutting has the same trend with shear angle, friction angle and shear stress obtained from orthogonal cutting. Moreover, transformation oblique force coefficients from orthogonal tests contain small error percentages, 10% and 7% in feed and tangential directions respectively, however in radial direction average of 25% error obtained which relatively high compared to feed and tangential directions.

- Chip flow angle is one of the critical parameters in oblique cutting. In this study, it is determined by 3 different methods: Stabler's chip flow rule, experimentally and analytical prediction. Oblique cutting force coefficients are determined and compared with the transformed cutting coefficients from orthogonal cutting tests for different chip flow angle measurement methods. It is observed that the analytical prediction of chip flow angle yield better results than the other two methods.

In Chapter 4, an investigation of the edge forces and the hone radius effect on the cutting process are conducted. An initial analytical model which is proposed by Ozlu [20] is applied for orthogonal cutting. The analytical approach takes the measured flank contact as inputs and predicts the machining forces in the presence of a honed cutting tool. Promising agreement is obtained between the analytical solution and experimental results. Following are the specific observations:

- The total cutting forces increase non-linearly with the increasing hone radius. However a 100% increase in hone radius results in about 5% and 10% increase in feed and tangential forces, respectively.

- Similarly, the edge cutting forces increase non-linearly with the increasing hone radius. 100% increase in hone radius results in about 8% and 14% increase in feed and

tangential edge forces at large hone radius values. However, at small hone radius values the percentage increments are 36% and 40%, for the feed and tangential edge forces respectively.

- It is observed that the total cutting forces decrease with increasing clearance angle. The effect of the clearance angle on the feed forces is more drastic than on the tangential forces.
- It is shown experimentally that 3 times increase in clearance angle decreases the flank contact length by half.

To conclude, in this thesis the orthogonal cutting and oblique cutting mechanics are investigated analytically and experimentally for different cutting conditions. During these investigations it is once again showed that, feed rate, cutting speed and tool geometry has a great influence on important cutting parameters such as shear angle, friction angle, shear angle and chip flow angle in oblique cutting. For chip flow angle, the analytical results yield the lowest percentage error, therefore better results can be obtained if it is used in oblique transformation instead of Stabler's chip flow law Also, it is shown that oblique transformation methods can be applied in orthogonal cutting in order to predict the cutting forces in oblique cutting. On the other hand, edge cutting forces in orthogonal cutting are modeled by considering the hone radius effect and promising agreement is obtained between the analytical solution and experimental results. For future work, this study can be extended for different materials and cutting conditions and the chip flow angle measurement in oblique cutting can be improved by using more sensitive equipment during cutting. Also, the effect of hone radius in oblique cutting can be investigated and edge cutting force prediction model can be extended for oblique cutting.

REFERENCES

[1] Merchant, E., 1945, Mechanics of the Metal Cutting Process I. Orthogonal Cutting and a Type 2 Chip, Journal of Applied Physics, 16/5:267-275.

[2] E.H. Lee and B.W. Shaffer, 1951, The Theory of plasticity applied to a problem of machining, Trans. ASME, J. Appl. Mech., 18:405–413.

[3] Palmer, W.B., Oxley, P.L.B., 1959, Mechanics of Orthogonal Machining, Proc. Instn. Mech. Engrs., 173/24:623-638.

[4] Krystof, J., 1939, Berichte uber Betriebswissenschafliche Arbeiten, Bd., 12. VDI Verlag.

[5] M. C. Shaw, N.H. Cook, and I. Finnie, 1953, The Shear-Angle Relationship in Metal Cutting", Transaction ASME, 75:273-283.

[6] G. V. Stabler, 1964, The Chşp Flow Law and Its Consequences. Advances ,n Machine Tool Design and Research, pp.243-251

[7] Altintas, Y., 2000, Manufacturing Automation, Cambridge University Press.

[8] Armarego, E.J.A., Brown, R.H., 1969, "*The Machining of Metals*", Prentice-Hall.

[9] Yen, Y., Jain, A., Altan, T, 2004, A finite element analysis of orthogonal machining using different tool edge geometries, J. Mat. Proc. Tech., 146:72-81.

[10] Waldorf D. A, 2006, Simplified Model for Ploughing Forces in Turning, Journal of Manufacturing Processes, 8/ 2, 2006, 76-82.

[11] Hsu T.C., A study of the shear and normal stresses on a cutting tool, Transactions of ASME, Journal of Engineering for Industry 88, 1966, 51–54.

[12] Shatla M., Yen Y.C., Altan T., Tool-workpiece interface in orthogonal cutting—application of FEM modeling, Transactions of NAMRI/SME 28, 2000, 173–178.

[13] Waldorf D.J., DeVor R.E., Kapoor S.G., A slip-line field for ploughing during orthogonal cutting, Transactions of ASME, Journal of Manufacturing Science and Engineering 120, 1998, 693–699.

[14] Waldorf D.J., A simplified model for ploughing forces in turning, Transactions of NAMRI/SME 32, 2004, 447–454.

[15] Fang N., Slip-line Modeling of Machining with a Rounded Edge Tool-Part I: New Model and Theory, Journal of Mechanics and Physics of Solids, 51, 2003, 715-742.

[16] Wu D.W., Application of a Comprehensive Dynamic Cutting Force Model to Orthogonal Wave Generating Processes, International Journal of Mechanical Science, 30/8, 1988, 581-600.

[17] Manjunathaiah J., Endres W.J., A new model and analysis of orthogonal machining with an edge-radiused tool, Transactions of ASME 122, 2000, 384–390.

[18] Manjunathaiah J., Endres W.J., A study of apparent negative rake angle and its effects on shear angle during orthogonal cutting with edge-radiused tools, Transactions of NAMRI/SME 28, 2000, 197–202.

[19] Ranganath S.,Campbell A.B.,Gorkiewicz D.W, A model to calibrate and predict forces in machining with honed cutting tools or inserts. International Journal of Machine Tools and Manufacture, 47, 2007, 820-840.

[20] Ozlu E., 2008, Analytical Modeling of Cutting Process Mechanics and Dynamics for Simulation of Industrial Machining Operations, PhD Thesis, FENS Sabanci University, Istanbul.

[21] Molinari, A., and Dudzinski, D., Stationary shear bands in high speed machining, Comptes Rendus Acad. Sciences, 315, Série II, 1992, 399-405.

[22] Moufki, A., Molinari, A., and Dudzinski, D., Modelling of Orthogonal Cutting with a Temperature Dependent Friction Law, J. Mech. Phys. Solids, 46/10, 1998, 2103-2138.

[23] Zorev, N. N., Inter-relationship between shear processes occurring along tool face and shear plane in metal cutting, International Research in Production Engineering, ASME, New York, 1963, 42-49.

[24] Lo, S.P., Lin, Y., An investigation of sticking behavior on the chip-tool interface using thermo-elastic-plastic finite element method, J Mat. Proc. Tech., 121, 2002, 285-292.

[25] Atkins, A.G., Toughness and Oblique Metalcutting. Journal of Manufacturing Science and Engineering, Vol.128, pp.775-786.

[26] Kato, S., Yamaguchi, K., and Yamada, M., Stress Distribution at the Interface Between Tool and Chip in Machining, Journal of Eng. for Industry, 94, 1972, 683-689.

[27] Barrow, G., Graham, T., Kurimoto, T., and Leong, F., Determination of Rake Face Stress Distribution in Orthogonal Machining, Int. J. Mach. Tool. Des. Res., 22/1, 1982, 75-85.

[28] Ozlu, E., Budak E., Development of a Thermomechanical Cutting Process Model for Machining Process Simulations, Annals of the CIRP, 57, 2008, 97-100.

[29] Schimmel R. J., Manjunathaiah J., Endres W.J. Edge radius variability and force measurement considerations, Journal of Manufacturing Science and Engineering, 122/3, 2000, 590-593.

[30] Bil H., Kılıç S.E., Tekkaya E.A., A comparison of orthogonal cutting data from experiments with three different finite element models, International Journal of Machine Tools and Manufacture, 44/9, 2004, 933-944.

[31] Powell, M. J. D., "A Fortran Subroutine for Solving Systems of Nonlinear Algebraic Equations," Numerical Methods for Nonlinear Algebraic Equations, P. Rabinowitz, ed., Ch.7, 1970.

[32] Jaspers, S.P.F.C., Dautzenberg, J.H., 2002, Material Behaviour in conditions similar to metal cutting: flow stress in the primary shear zone, Journal of Materials Processing Technology, 122: 322-330.

[33] Kalpakjian, S. Manufacturing Engineering and Technology. Addison-Wesley, 1995.

APPENDIX

Rake Angle (deg)	Test	Cutting Speed (m/min)	Feed Rate (mm/rev)	Cut Chip Thickness (mm)	Feed Force (N)	Tangential Force (N)	Shear Angle (deg)	Friction Angle (deg)	Shear Stress (MPa)	K_{fc} (MPa)	K_{tc} (MPa)
0	1	60	0.1	0.27	500	620	18	30	552	1275	2185
	2	60	0.15	0.36	600	825	23	29	584	1183	2140
	3	60	0.2	0.41	675	1000	24	28	600	1075	2043
	4	60	0.25	0.47	750	1180	26	27	603	1010	1994
	5	150	0.1	0.21	340	520	23	19	671	665	2050
	6	150	0.15	0.27	390	700	27	18	688	610	1967
	7	150	0.2	0.35	450	900	29	17	701	608	1975
	8	150	0.25	0.41	500	1100	30	16	720	586	1980
	9	250	0.1	0.18	300	475	25	17	616	525	1765
	10	250	0.15	0.26	350	625	28	17	599	517	1677
	11	250	0.2	0.32	385	800	29	16	628	475	1870
	12	250	0.25	0.39	425	1000	30	15	663	460	1756
	13	400	0.1	0.17	270	470	28	23	595	725	1795
	14	400	0.15	0.24	320	655	30	21	631	650	1813
	15	400	0.2	0.33	420	870	31	20	643	600	1723
	16	400	0.25	0.39	400	980	32	20	571	550	1738
5	17	60	0.1	0.30	395	550	20	29	566	950	2155
	18	60	0.15	0.38	450	775	24	25	645	817	2187
	19	60	0.2	0.44	515	950	27	25	662	775	2078
	20	60	0.25	0.54	550	1100	28	24	639	690	1962
	21	150	0.1	0.22	328	500	25	22	654	625	1995
	22	150	0.15	0.28	375	690	28	21	697	573	1957
	23	150	0.2	0.37	410	870	29	20	697	518	1918
	24	150	0.25	0.47	470	1050	30	20	696	534	1934
	25	250	0.1	0.21	305	515	27	21	674	555	1965
	26	250	0.15	0.27	335	680	30	19	708	470	1910
	27	250	0.2	0.34	360	870	31	18	719	415	1870
	28	250	0.25	0.42	380	1040	32	16	721	372	1836
	29	400	0.1	0.19	300	505	29	22	725	615	2060
	30	400	0.15	0.25	320	670	32	19	746	510	1973
	31	400	0.2	0.34	385	865	32	20	720	520	1930
	32	400	0.25	0.38	370	1020	35	19	721	456	1854

Table A-1: AISI 4340 orthogonal cutting test results

rake angle (D)	cutting speed (m/min)	feed (mm/rev)	Feed Force (N)	Tangent. Force (N)	chip ratio	shear angle (D)	friction angle (D)	shear stress (MPa)	Kfc (MPa)	Ktc (MPa)	Kfe (N/mm)	Kte (N/mm)
-5	3	0.06	220	330	0.43	22	22	449	806	1605	54	57
	3	0.12	320	550	0.52	27	21	504	791	1655	54	57
	3	0.18	425	750	0.59	29	21	499	798	1620	54	57
	6	0.06	210	315	0.45	23	18	498	698	1667	56	47
	6	0.12	300	520	0.58	29	18	524	698	1628	56	47
	6	0.18	390	740	0.64	31	18	545	698	1654	56	47
	10	0.06	200	300	0.49	25	19	506	736	1659	49	40
	10	0.12	285	500	0.62	30	18	522	698	1605	49	40
	10	0.18	385	720	0.75	35	19	531	724	1638	49	40
-10	3	0.06	245	350	0.43	21	17	509	930	1860	58	51
	3	0.12	375	580	0.47	23	18	507	969	1822	58	51
	3	0.18	490	825	0.54	26	17	546	943	1848	58	51
	6	0.06	240	330	0.43	22	14	479	775	1705	65	51
	6	0.12	360	560	0.56	27	16	528	853	1744	65	51
	6	0.18	450	775	0.64	30	15	543	801	1718	65	51
	10	0.06	240	320	0.53	26	19	518	1008	1814	51	40
	10	0.12	350	540	0.72	32	18	529	930	1760	51	40
	10	0.18	490	780	0.67	30	19	531	982	1793	51	40

Table A-2: Ti_6Al_4V titanium alloy orthogonal cutting test results with clearance angle 5°

rake angle (D)	cutting speed (m/min)	feed (mm/rev)	Feed Force (N)	Tangent. Force (N)	chip ratio	shear angle (D)	friction angle (D)	shear stress (MPa)	Kfc (MPa)	Ktc (MPa)	Kfe (N/mm)	Kte (N/mm)
0	3	0.06	190	310	0.51	27.0	26.6	420	698	1395	47	60
	3	0.12	240	550	0.55	28.9	18.4	562	543	1628	47	60
	3	0.18	350	700	0.68	34.2	23.7	481	646	1473	47	60
	6	0.06	180	300	0.48	25.6	19.3	503	543	1550	51	47
	6	0.12	250	500	0.56	29.2	19.3	531	543	1550	51	47
	6	0.18	320	700	0.61	31.2	19.3	541	543	1550	51	47
	10	0.06	200	300	0.57	29.5	21.6	516	612	1550	56	47
	10	0.12	265	500	0.62	31.9	19.8	540	558	1550	56	47
	10	0.18	350	700	0.76	37.3	20.9	530	592	1550	56	47
3	3	0.06	170	300	0.45	24.8	18.1	516	419	1550	54	47
	3	0.12	220	500	0.57	30.5	17.6	574	403	1550	54	47
	3	0.18	275	700	0.59	31.4	17.8	578	411	1550	54	47
	6	0.06	225	300	0.5	26.9	18.1	540	419	1550	80	47
	6	0.12	275	500	0.62	32.6	17.6	586	403	1550	80	47
	6	0.18	330	700	0.65	33.7	17.8	589	411	1550	80	47
	10	0.06	225	300	0.63	32.8	20.2	614	519	1682	73	39
	10	0.12	275	400	0.68	35.1	23.3	428	453	1229	73	39
	10	0.18	350	675	0.7	36.1	21.0	556	496	1530	73	39

	3	0.06	220	300	0.56	30.4	15.6	609	264	1550	87	47
	3	0.12	250	500	0.57	31.3	15.1	621	248	1550	87	47
	3	0.18	285	700	0.61	33.0	15.4	633	256	1550	87	47
	6	0.06	200	300	0.51	28.3	18.3	548	326	1488	73	50
6	6	0.12	225	425	0.64	34.4	17.9	490	260	1229	73	50
	6	0.18	275	650	0.65	34.9	18.2	558	302	1401	73	50
	10	0.06	220	285	0.57	31.1	18.2	537	302	1395	84	49
	10	0.12	265	475	0.67	35.5	18.8	568	326	1434	84	49
	10	0.18	300	650	0.75	38.9	18.3	567	307	1408	84	49
	3	0.06	200	320	0.6	33.8	20.9	404	194	1240	81	74
	3	0.12	225	500	0.66	36.9	20.4	432	194	1318	81	74
	3	0.18	250	650	0.77	41.8	20.7	394	194	1266	81	74
	6	0.06	210	300	0.63	35.1	18.2	469	147	1357	89	58
12	6	0.12	235	475	0.69	38.0	19.2	456	171	1357	89	58
	6	0.18	250	650	0.69	38.3	18.4	464	152	1357	89	58
	10	0.06	220	275	0.63	35.4	16.5	534	116	1488	95	39
	10	0.12	235	450	0.75	41.0	16.7	501	116	1422	95	39
	10	0.18	250	650	0.85	45.1	16.5	495	116	1465	95	39

Table A-3: Ti_6Al_4V titanium alloy orthogonal cutting test results with clearance angle 5°

oblique angle (D)	cutting speed (m/min)	feed (mm/rev)	Feed Force (N)	Tangent. Force (N)	Radial Force (N)	Chip flow (D)	chip ratio	shear angle (D)	friction angle (D)	shear stress (MPa)	Kfc (MPa)	Ktc (MPa)	Krc (MPa)
7	3	0.06	180	300	30	7.5	0.54	28	23	553	612	1659	155
	3	0.12	265	540	50	8.2	0.61	31	21	608	636	1760	155
	3	0.18	340	740	70	7.8	0.57	30	19	574	618	1690	155
	6	0.06	190	310	30	6.8	0.58	30	20	508	612	1527	171
	6	0.12	255	500	55	6.5	0.74	37	19	521	558	1500	182
	6	0.18	340	700	75	6.6	0.74	37	18	516	592	1517	173
	10	0.06	195	290	35	6.2	0.59	30	22	532	659	1605	171
	10	0.12	270	490	60	7	0.76	37	21	533	620	1578	182
	10	0.18	360	700	80	7.2	0.71	35	22	537	646	1594	173
11	3	0.06	180	315	45	9.2	0.56	29	22	551	651	1667	194
	3	0.12	260	540	80	9.1	0.59	31	21	579	636	1705	233
	3	0.18	345	750	100	9.6	0.64	33	21	572	643	1680	207
	6	0.06	190	300	40	9.8	0.52	27	22	511	612	1581	155
	6	0.12	255	510	80	10.2	0.63	32	19	563	558	1605	233
	6	0.18	340	710	90	11	0.63	32	21	544	592	1587	181
	10	0.06	195	310	40	9.3	0.57	30	24	476	659	1488	171
	10	0.12	250	485	75	8.8	0.84	40	21	476	543	1422	221
	10	0.18	350	685	90	9.8	0.68	34	23	483	620	1465	186

TableA-4: Ti_6Al_4V titanium alloy oblique cutting test results with clearance angle 5°